Turun yliopisto
University of Turku

SPIN POLARIZATION AND NORMAL REFLECTION AT NANOSCALE POINT CONTACTS

Elina Tuuli

TURUN YLIOPISTON JULKAISUJA – ANNALES UNIVERSITATIS TURKUENSIS
Sarja - ser. AI osa - tom. 506 | Astronomica - Chemica - Physica - Mathematica | Turku 2015

University of Turku

Faculty of Mathematics and Natural Sciences

Department of Physics and Astronomy

Supervised by

Prof. Kurt Gloos
Wihuri Physical Laboratory
Dept. of Physics and Astronomy
University of Turku
Turku, Finland

Reviewed by

Prof. Gernot Goll
Karlsruher Institut für Technologie (KIT)
DFG Center for Functional
Nanostructures (CFN)
Wolfgang-Gaede-Str. 1a
76131 Karlsruhe, Germany

Prof. Ilari Maasilta
Department of Physics
P.O. Box 35 (YFL)
40014 University of Jyväskylä
Finland

Opponent

Prof. Yurii G. Naidyuk
Department of Point-Contact Spectroscopy
B. Verkin Institute for Low Temperature
Physics and Engineering
Lenin Ave. 47
61103 Kharkiv
Ukraine

The originality of this thesis has been checked in accordance with the University of Turku quality assurance system using the Turnitin OriginalityCheck service.

ISBN 978-951-29-6011-8 (PRINT)

ISBN 978-951-29-6012-5 (PDF)

ISSN 0082-7002

Painosalama Oy - Turku, Finland 2015

Acknowledgements

This work has been carried out in the Wihuri Physical Laboratory at the Department of Physics and Astronomy at University of Turku. The Jenny and Antti Wihuri Foundation, the National Doctoral Programme in Nanoscience, the Graduate School of Materials Research, The Finnish Concordia Fund and Professor Väinö Hovi Fund are acknowledged for financial support.

I wish to thank Prof. I. Maansilta and Prof. G. Goll for reviewing this thesis and Prof. Yu. G. Naidyuk for being my opponent at the dissertation. I would also like to thank Prof. K. Gloos for supervision during the process that led to this moment. I also thank Prof. P. Paturi for her advice and all my co-workers for the interesting discussions over the years.

I would like to thank my family for their love, caring and support, and all of my friends for their company. Discussing, joking, running, hiking and simply being with you has been utterly important for me. Thank you for sharing the happy moments and holding my hand through the difficult ones. Special thanks to A. Kosonen for proof reading.

Turku, January 2015

Elina Tuuli

Abstract

This thesis presents point-contact measurements between superconductors (Nb, Ta, Sn, Al, Zn) and ferromagnets (Co, Fe, Ni) as well as non-magnetic metals (Ag, Au, Cu, Pt). The point contacts were fabricated using the shear method. The differential resistance of the contacts was measured either in liquid He at 4.2 K or in vacuum in a dilution refrigerator at varying temperature down to 0.1 K. The contact properties were investigated as function of size and temperature. The measured Andreev-reflection spectra were analysed in the framework of the BTK model – a three parameter model that describes current transport across a superconductor - normal conductor interface. The original BTK model was modified to include the effects of spin polarization or finite lifetime of the Cooper pairs.

Our polarization values for the ferromagnets at 4.2 K agree with the literature data, but the analysis was ambiguous because the experimental spectra both with ferromagnets and non-magnets could be described equally well either with spin polarization or finite lifetime effects in the BTK model. With the polarization model the Z parameter varies from almost 0 to 0.8 while the lifetime model produces Z values close to 0.5. Measurements at lower temperatures partly lift this ambiguity because the magnitude of thermal broadening is small enough to separate lifetime broadening from the polarization. The reduced magnitude of the superconducting anomalies for Zn-Fe contacts required an additional modification of the BTK model which was implemented as a scaling factor. Adding this parameter led to reduced polarization values. However, reliable data is difficult to obtain because different parameter sets produce almost identical spectra.

Tiivistelmä

Tässä väitöskirjassa esitellään pistekontaktimittauksia suprajohteiden (Nb, Ta, Sn, Al, Zn) ja ferromagneettien (Co, Fe, Ni) sekä ei-magneettisten metallien (Ag, Au, Cu, Pt) välillä. Kontaktit luotiin ristikkäisten metallilankojen väliin, ja niiden differentiaalinen resistanssi mitattiin joko nestemäisessä heliumissa 4.2 kelvinin lämpötilassa tai tyhjiössä jopa 0.1 kelvinissä. Kontaktien ominaisuuksia tutkittiin sekä niiden koon että mittauslämpötilan funktiona. Mitatut Andreevin heijastusspektrit analysoitiin muokatuilla BTK-malleilla, jotka kuvaavat virran kulkua suprajohde – normaali metalli -rajapinnan läpi ja huomioivat sekä spinpolarisaation että Cooperin parien äärellisen elinajan vaikutuksen.

4.2-asteisessa nestemäisessä heliumissa saadut polarisaatioarvot olivat yhtäpitäviä kirjallisuusarvojen kanssa, mutta koska kokeelliset spektrit oli mahdollista sovittaa sekä spinpolarisaation että äärellisen elinajan aiheuttamien vaikutusten avulla, analyysi oli monitulkintainen. Kun spektrit sovitettiin polarisaatiota käyttäen, Z-parametri vaihteli välillä 0 – 0.8, mutta Cooperin parien elinaikaa käytettäessä arvot keskittyivät lähelle arvoa 0.5. Matalammissa lämpötiloissa tulkinnallisuus väheni, koska Cooperin parien elinajan aiheuttama spektrin leviäminen voitiin erottaa lämpötilan vaikutuksesta.

Zn-Fe-kontakteista mitattujen spektrien suprajohtavien anomalioiden havaittiin kuitenkin olevan matalissa lämpötiloissa tavallista pienempiä, ja sitä selittämään BTK-mallia muokattiin lisäämällä siihen vielä skaalauskerroin. Tämän parametrin käyttäminen johti pienempiin polarisaatioarvoihin. Tässä tapauksessa spektrit oli mahdollista kuvata useilla eri parametrijoukoilla, mikä vaikeutti luotettavan datan saamista.

List of Publications

This thesis is based on the experimental work carried out at the Wihuri Physical Laboratory, Department of Physics, University of Turku during the years 2010-2013. The thesis consists of an introductory part and of the following publications:

[**P1**] E. Tuuli and K. Gloos: *Andreev-reflection spectroscopy of ferromagnets: the impact of Fermi surface mismatch*, Low Temperature Physics **37**, 485 (2011) [Fizika Nizkikh Temperatur **37**, 609 (2011)].

[**P2**] E. Tuuli and K. Gloos: *Spin polarization versus lifetime effects at point contacts between superconducting niobium and normal metals*, Journal of Physics Conference Series **400**, 042065 (2012).

[**P3**] E. Tuuli and K. Gloos: *Normal reflection at superconductor - normal metal interfaces due to Fermi surface mismatch*, Journal of Physics Conference Series **400**, 042066 (2012).

[**P4**] K. Gloos and E. Tuuli: *Electron and hole transmission through superconductor - normal metal interfaces*, Journal of the Korean Physical Society **62**, 1575 (2013).

[**P5**] E. Tuuli and K. Gloos: *Spin polarization and suppression of superconductivity at nanoscale ferromagnet - superconductor interfaces*, accepted for publication in Journal of Low Temperature Physics.

Articles relevant to this work but not included in this thesis

[**P6**] K. Gloos and E. Tuuli: *Break-junction experiments on the zero-bias anomaly of non-magnetic and ferromagnetically ordered metals*, Journal of Physics Conference Series **400**, 042011 (2012).

[**P7**] K. Gloos, J. Huupponen and E. Tuuli: *Phonon-drag induced suppression of the Andreev hole current in superconducting niobium contacts*, Journal of Physics Conference Series **400**, 042010 (2012).

[**P8**] K. Gloos and E. Tuuli: *Andreev-reflection spectroscopy with superconducting indium - A case study*, Low Temperature Physics **39**, 252 (2013) [Fizika Nizkikh Temperatur **39**, 326 (2013)].

[**P9**] K. Gloos and E. Tuuli: *Mechanisms of normal reflection at metal interfaces studied by Andreev-reflection spectroscopy*, Fiz. Nizk. Temp. **40**, 1155 (2014).

Symbols and Abbreviations

Symbol	Units	Description
$\mathcal{A}$	m^2	Area
a	m	Contact radius
d	m	Contact diameter
Δ	eV	Superconducting energy gap
e	C	Electron charge
$\Gamma = \hbar/\tau$	eV	Lifetime parameter
G	$1/\Omega$	Conductance
$G_0 = 2e^2/h$	$1/\Omega$	Quantum conductance
H	A/m	Magnetic field strength
I	A	Current
$I(V)$		Current-voltage characteristics
k_F	1/m	Fermi wave length
k_B	J/K	Boltzmann constant
l	m	The mean free path of electrons
l_{el}	m	Elastic mean free path of electrons

l_{in}	m	Inelastic mean free path of electrons
μ	J/T	magnetic moment of electron
N	1/(eVm^3)	Density of states
N_s	1/(eVm^3)	Superconducting density of states
ρ	Ωm	Resistivity
n	1/m^3	Electron density
R_M	Ω	Maxwell resistance
R_{Sh}	Ω	Sharvin resistance
τ		Transmission coefficient
T	K	Temperature
T		Three dimensional transmission coefficient
τ	s	Quasiparticle lifetime
V	V	Voltage

Contents

1. Introduction

Point-contact spectroscopy is an experimental method that was invented in 1974 by I. K. Yanson who found non-linear features in the current voltage characteristics of a contact in a membrane between two metal films. The non-linearities were related to the electron-phonon scattering of the metals, and point-contact spectroscopy has since been used to investigate different properties of metals and contacts [1–3].

Differential resistance spectra of point contacts sometimes have additional anomalies at zero bias. Their origin is not known but one of the suggested explanations is Kondo scattering at impurities in the contact region. These anomalies can be either minima or maxima, and their shape corresponds to an impurity spin from 0.1 to 0.2 in units of $\hbar$. Such a spin could arise from a cloud of polarized conduction electrons trapped in the contact region [4, 5]. This polarization should be measurable with point-contact Andreev reflection spectroscopy which led to the experiments presented in this thesis.

The articles included in this thesis contain:

[P1] *"Andreev-reflection spectroscopy of ferromagnets: the impact of Fermi surface mismatch"* Spectra of contacts between superconductors Nb and $AuIn_2$ and normal conductors Co and Cu were analysed with two different modified BTK models - one that includes spin polarization and the other one the finite lifetime effects. We found that both models can describe the spectra of ferromagnetic Co and non-magnetic Cu equally well. We suggested more information on normal reflection and quasiparticle lifetime would be needed to resolve the degeneracy.

[P2] *"Spin polarization versus lifetime effects at point contacts between superconducting niobium and normal metals"* Contacts between superconducting Nb and the ferromagnets Co, Fe and Ni as well as the noble metals Ag, Cu and Pt support our previous results on the dual interpretation of the point-contact spectra.

[P3] *"Normal reflection at superconductor - normal metal interfaces due to Fermi surface mismatch"* The lifetime model analysis of spectra of superconductors Nb and Al in contact with non-magnetic normal metals Ag, Cu and Pt yielded Z parameters close to 0.5. The possibility that this represented the Fermi surface mismatch was discussed.

[P4] *"Electron and hole transmission through superconductor - normal metal interfaces"* Superconducting Al in contact with non-magnetic normal conductors Ag, Au, Cu, Pd and Pt to investigate the size dependence of the Z parameter. We discussed the possibility that Fermi surface mismatch did not cause the constant Z parameter.

[P5] *"Suppression of superconductivity at nanoscale ferromagnet - superconductor interfaces"* Ferromagnetic Fe in contact with superconductors Nb, Ta, Sn, Al and Zn to investigate the effect that the strength of the superconductor has on Andreev reflection and the extracted spin polarization. The analysis of the spectra shows that the superconductivity could be suppressed at the contact interface.

1.1 Techniques for measuring the spin polarization

Measuring spin polarization is important to a field known as spintronics, or spin electronics [6–9]. During recent years the electronic circuits in computers have become smaller and smaller, even down to nanoscale, and also data storage has become denser. Eventually the aim is to use not only the charge but also the spin of electrons to store information. Spintronics research includes topics ranging from the creation of spin polarized currents to defining its coherence length and measuring the polarization of the transmitted current.

Ferromagnetic materials can be characterized by the imbalance of spin up and spin down electrons at the Fermi level with the densities of electronic states presented in Figure 1.1. While their magnetization $M = \frac{N}{V}\mu$ can be uniquely defined with the difference of the amount of spin up and spin down electrons, $N = N_\downarrow - N_\uparrow$, with magnetic moment μ in volume V [10], there are many possible definitions for the spin polarization P of the material [11, 12].

Despite this, several methods for measuring the spin polarization have been proposed, including spin polarized photoemission [13, 14], spin-polarized tunneling [15] and Andreev reflection spectroscopy [16, 17]. These experimental techniques match

different theoretical definitions for the polarization and it can therefore be difficult to compare the polarization values extracted from them [11, 12]. It is expected that the polarization of non-magnetic metals should be equal to zero [18] and that half-metals with only one of the spin species at the Fermi level should have a spin polarization of one [11]. One of the most commonly appearing definitions is

$$P = \frac{N_\uparrow - N_\downarrow}{N_\uparrow + N_\downarrow} \tag{1.1}$$

where $N_{\uparrow,(\downarrow)}$ are the densities of states at the Fermi level, but this polarization can not be probed directly with all experimental methods because there are usually other mechanisms in addition to the effect of the densities of states that affect the current transport [11]. It is also possible to define the polarization by dividing the current into two parts that consist of majority and minority electrons

$$P = \frac{I_\uparrow - I_\downarrow}{I_\uparrow + I_\downarrow}\,, \tag{1.2}$$

where currents $I_{\uparrow,(\downarrow)}$ that consist of the majority and the minority electrons depend not only on the density of states but also the Fermi velocities of the materials $I_{\uparrow,(\downarrow)} \propto v_{F,\uparrow,(\downarrow)} N_{\uparrow,(\downarrow)}(E_F)$ [11, 16, 18].

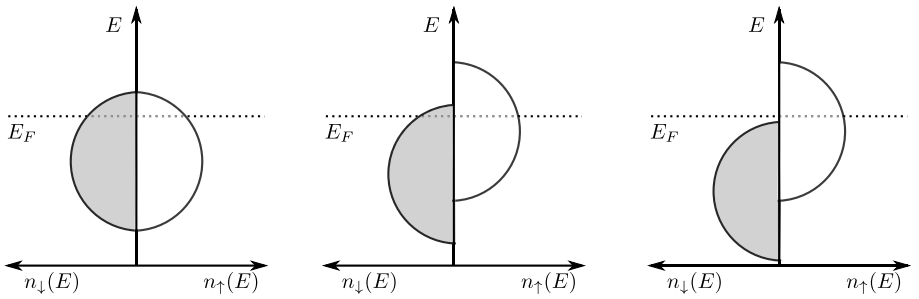

(a) Non-magnetic (b) Ferromagnetic (c) Half-metallic

Figure 1.1: Schematic representations of the electron densities of states of a) a non-magnetic metal, b) a ferromagnet and c) a half metal. For a non-magnetic metal there are equally many states for the spin up and down electrons at the Fermi level E_F, for a ferromagnet the number of spin up and down is not equal at the Fermi level and for a half metal only one of the spin species is present at the Fermi level.

1.1.1 Spin polarized photoemission

The spin of an electron is conserved in the photoemission process that consists of exciting an electron with a photon, after which the electron can diffuse to the surface and cross the surface barrier. The polarization of the ejected electrons according to Equation 1.1 can be measured with Mott scattering where an electron beam is scattered off of heavy atoms and the two spin species are scattered into different angles [19]. Spin polarized photoemission is sensitive to an approximately 2 nm thick surface layer and it can also be used to study the band structure of ferromagnets [14]. The first successful experiment was performed in 1969 by Busch *et al.* [14] who found that the spin polarization of Gd was approximately +5.5 %. Later also the polarization of Fe, Ni and Co has been measured [13]. The results are tabulated in Table 2.1.

1.1.2 Spin polarized tunneling

Tunnel junctions consist of two metals separated by a tunnel barrier and have been used widely to investigate properties of superconductors [20, 21] and also to measure the spin polarization of magnetic metals since 1971 [15, 22, 23].

When a magnetic field H is applied in the plane of the junction, the superconducting density of states $N_s(E)$ spin-splits by $2\mu H$, where μ is the magnetic moment of the electron. This was first observed in Al-Al_2O_3-Ag tunnel junctions by Meservey *et al.* [24] in 1970. Because a Cooper pair consists of two electrons in states $k_\uparrow$ and $-k_\downarrow$ also when a magnetic field is applied, one of the spin species will be lifted in energy by μH and the other will be lowered by μH. As the excited quasiparticle states are Δ apart from the paired ground state, the tunneling current at $\Delta - \mu H$ will consist of quasiparticles of one spin and the others at $-\Delta + \mu H$ of the other spin direction [15].

A ferromagnetic normal conductor can produce a spin polarized current which leads to an asymmetric tunneling conductance in magnetic field. This asymmetry contains information on the relative density of states in the ferromagnet, and thereby the spin polarization of the current.

1.1.3 Point-contact Andreev reflection spectroscopy

A third way to measure the spin polarization is point-contact Andreev reflection spectroscopy which utilizes nanoscale point-contacts between a superconductor and a normal conductor. Transporting current across such an interface requires the single electrons of the normal metal to be transformed to Cooper pairs in the superconductor. This

process is affected by the imbalance of spin up and down electrons in the normal metal. Point-contact Andreev reflection spectroscopy will be discussed in more detail in the next two chapters.

2. Point-contact spectroscopy

2.1 Point contacts

Point contacts are nanoscale constrictions between two conductors. Three different schematic views of contacts shaped as an orifice, a long channel and a cavity are presented in Figure 2.1. The shape of the contact does not have a large effect on their electronic properties [1]. Our experimental conditions are most likely closest to Figure 2.1c as the point contacts are formed between two macroscopic wires.

There are many experimental methods to form nanoscale point contacts. Some of them are simple while others require complicated nanolithographical procedures. Among the earliest point-contact measurements were pressure contacts between two wires [25] and pinholes in tunnel junctions [1, 2]. A schematic view of the latter case is presented in Figure 2.2a. Such holes can form accidentally when making tunnel junctions if the oxide layer is not thick enough but they can also be fabricated intentionally by reducing the depth of the oxide layer, with a sharp needle, or by applying an electric field to break the weakest part of the insulating layer. A hole can also be etched into the dielectric membrane and the two conducting films grown on both sides afterwards. Contacts of this kind are usually very stable with respect to thermal and mechanical variations, and can therefore be easily used to measure point contacts as function of temperature or magnetic field [1].

Point contacts can also be constructed mechanically, for example with a so called spear-anvil method shown in Figure 2.2b. The contact is formed by pressing a sharp tip (spear) against a flat electrode (anvil). Jansen *et al.* [26] were the first ones to fabricate contacts of this type. The area of the tip is typically larger than that of the individual contacts and after a set of measurements it is typically deformed. The tip can be moved with a differential screw mechanism that allows controlled changes of both the position and size of the contact interface. Contacts of this kind often have some oxides or, if prepared in ambient conditions, a layer of water molecules at the interface. This can

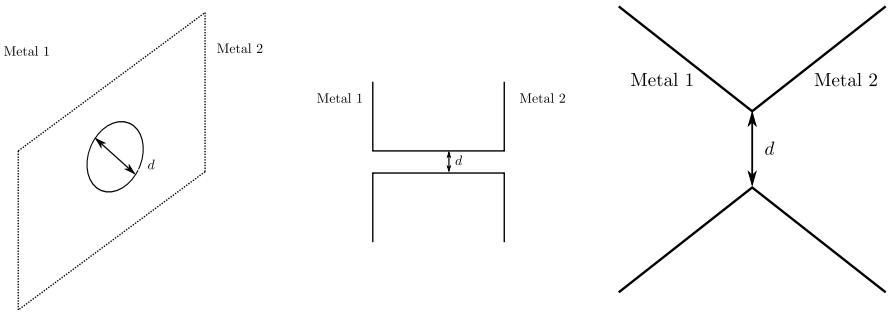

(a) An orifice between films. (b) A long channel. (c) A cavity.

Figure 2.1: Schematic views of point contacts characterized with a diameter d: a) a circular orifice in an insulating layer between two metal films, b) a long channel of length L much longer than the diameter d, and c) a cavity.

show in the spectra as tunneling-like features but often such a layer is broken when the contact is formed [1, 2, 27]. Contacts of this kind can also be manufactured with a scanning tunneling microscope which enables more spatial accuracy [2].

The spear-anvil technique can be modified to form contacts between two crossed wires or rods as shown in Figure 2.2c. This is known as the shear (or crossed-wire) method. The wires can slide against each other which should lead to less deformations to the material than with the spear-anvil method while cleaning the contact area of oxides and impurities. Also in this case the position and size of the contacts can be varied *in situ* [1].

Wires can also be used to form point-contact interfaces through mechanically controllable break junctions. A notch is cut to a wire that has been attached to a bending beam as shown in Figure 2.2d. When the beam is bent, the wire will break into two at the position of the notch. When done at low temperatures in vacuum, this will expose clean metal surfaces that can be pressed back together to form a contact. The point contacts made with this method are mechanically so stable that they have been applied to investigate atomic size contacts but are limited to having the same metal as both electrodes [1, 27].

2.2 Point-contact spectroscopy

To start understanding scattering processes at point contacts, one can begin with a free-electron-like picture and think of electrons as individual particles flying through and

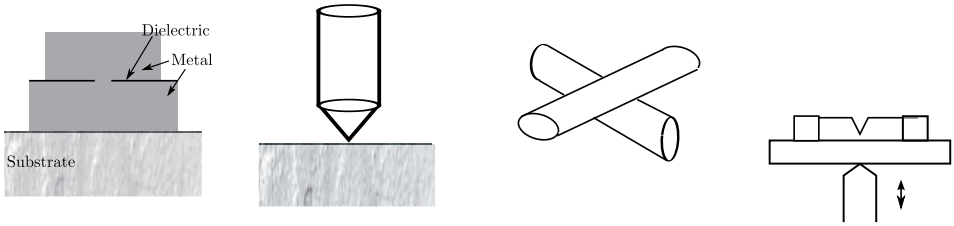

(a) A contact between two films. (b) A spear-anvil contact. (c) A shear-method contact. (d) A break junction.

Figure 2.2: A schematic representation of different methods used to fabricate point contacts: a) as a hole in an insulator between two thin films, b) by pressing a needle (spear) to a film (anvil) and a wire (anvil), c) by gently touching two wires and d) by breaking a wire.

scattering in the background created by the ions. Though in many of the theoretical works describing the observed phenomena more advanced models are used, this simplification allows useful insight into the topic.

In electronic equilibrium, the Fermi levels of the electrodes are aligned. If they consist of the same material, this is a natural assumption. For contacts between different metals this is accomplished by changing the zero point of the energy as shown in Figure 2.3a. Biasing the contact with a voltage lifts one of the electrodes to a higher potential (Figure 2.3b). This accelerates the electrons travelling through the contact because when they cross the contact interface, their energy is eV higher than that of the unbiased electrode [1].

Point contacts can be used to probe how the electrons scatter with different quasiparticles as function of energy. If the electrons scatter with these particles, they can be reflected back through the contact (Figure 2.4), leading to an excited quasiparticle with a maximum energy of eV. The quasiparticles can receive this energy only when it is equal to the energy of a transition to an excited state and hence the current through the contact is reduced at this specific voltage. These deviations are more easily observed in the first and second derivative of the current-voltage characteristics.

2.3 Transport regimes

A point contact is characterized by two lengths: the contact diameter, d, and the mean free path of electrons, l. The mean free path splits up to an elastic and inelastic con-

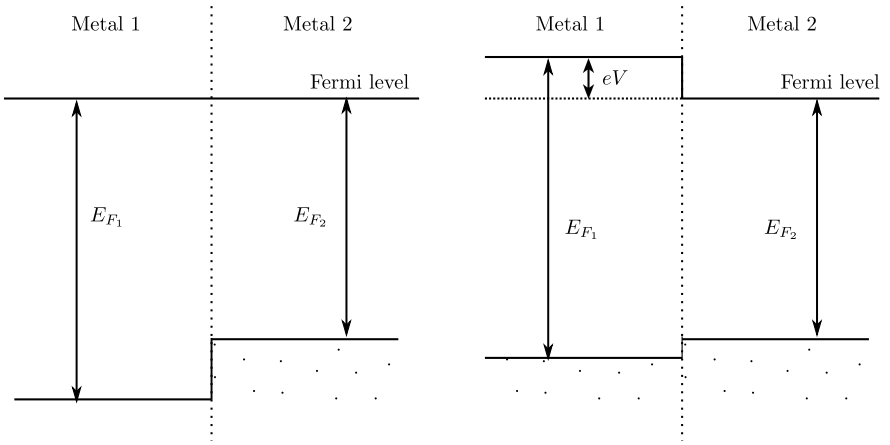

(a) In equilibrium. (b) Biased

Figure 2.3: The Fermi energies of a point contact between different materials both in equilibrium and biased with voltage V.

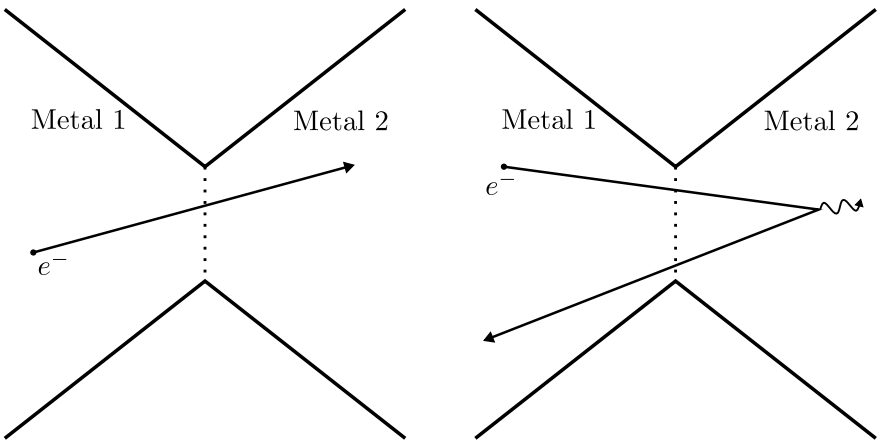

(a) No back scattering. (b) A back scattering event

Figure 2.4: Electrons can a) pass the contact region without scattering or b) they can scatter with, for example, phonons and be reflected back through the contact.

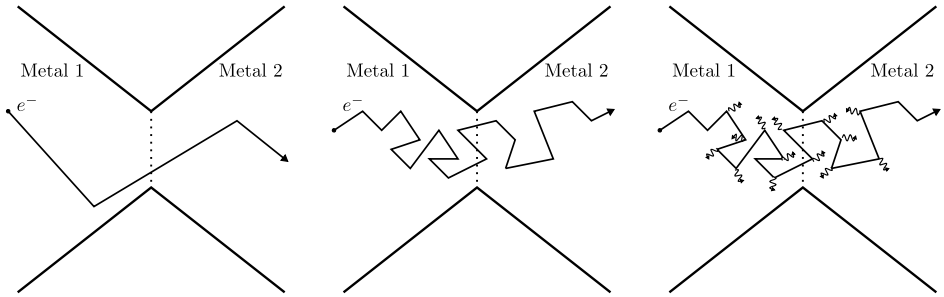

(a) The ballistic regime (b) The diffusive regime (c) The thermal regime

Figure 2.5: The three different transport regimes: a) ballistic with $l \gg d$, b) diffusive with $l_{el} \ll d \ll \sqrt{l_{in} l_{el}}$ and c) thermal with $l_{el}, l_{in} \ll d$.

tribution l_{el} and l_{in}, with $\frac{1}{l} \approx \frac{1}{l_{el}} + \frac{1}{l_{in}}$ according to the Matthiessen rule. These can be used to categorize the contacts into three transport regimes illustrated in Figure 2.5 called ballistic, diffusive, and thermal.

2.3.1 Ballistic transport regime

In the ballistic regime both of the mean free paths are much longer than the contact diameter, $l_{el}, l_{in} \gg d$. This means that the electrons flow through the contact without scattering in the contact region, as seen in Figure 2.5a. Therefore they dissipate their energy far from the contact and there should not be heating at the contact.

Ballistic electrons are accelerated at the contact interface and the increase in velocity, Δv, depends on the applied voltage as $\Delta v = eV/\hbar k_F$, where k_F is the Fermi wave number. The resistance of a ballistic point contact, derived by Yu. Sharvin in 1965 [28], is

$$R_{Sh} = \frac{16\rho l}{3\pi d^2}\,, \tag{2.1}$$

where ρ is the resistivity of the material, l is the mean free path of electrons, the product $\rho l = \hbar k_F / n e^2$ is a material specific constant of order $10^{-15}\Omega\mathrm{m}^2$, and n the electron density. This equation can be used to estimate the diameter d of the ballistic contacts. For Cu the diameter becomes approximately

$$d \approx 30\mathrm{nm}/\sqrt{R_{Sh}(\Omega)}\,. \tag{2.2}$$

This can be used as a rough estimate for most simple metals [1, 2] but it will not hold for very small contact interfaces because Equation 2.1 is correct only for $R \ll h/(2e^2) \approx 13\ \mathrm{k}\Omega$ as is described in Section 2.4.

Most pure metals have so long electron mean free paths that it is possible to fabricate ballistic point contacts with them. Many alloys and compound materials on the other hand have much shorter mean free paths which causes restrictions to the use of point-contact spectroscopy [1].

2.3.2 Thermal transport regime

In the thermal regime shown in Figure 2.5c the elastic and inelastic mean free paths are shorter than the contact diameter $l_{el}, l_{in} \ll d$. The resistance of a point contact in the thermal regime is obtained from Maxwell's formula

$$R_M = \frac{\rho}{d}\,. \tag{2.3}$$

This was derived by J. C. Maxwell by solving the Poisson equation for a circular orifice when the Ohm's law $\mathbf{j} = \sigma E$ is valid [1, 2].

Because of the amount of the scattering events in the contact region most of the energy carried by the electrons is dissipated in the contact volume. This can lead to significant Joule heating with the highest possible temperature at the centre of the contact, T_{max}, described by the Kohlrausch formula [29]

$$T_{max}^2 = T_{bath}^2 + \frac{V^2}{4L}\,, \tag{2.4}$$

where T_{bath} is the temperature of the environment of the point contact, V is the applied voltage, and $L = \pi^2 k_B^2/3e^2$ is the Lorenz number. When the bath temperature is much lower than the temperature of the point contact, the voltage dependence of the temperature can be estimated to be linear as

$$eV = \frac{2\pi}{\sqrt{3}} k_B T\,. \tag{2.5}$$

Because of the strong heating - at high voltages even large enough to raise the temperature of the point contact above room temperature - also the temperature-dependent resistivity $\rho(T)$ of the material affects the current-voltage characteristics [1, 3].

2.3.3 Diffusive transport regime

Between the ballistic and thermal regimes, where $l_{el} \ll d \ll \sqrt{l_{in} l_{el}}$, lies the diffusive transport regime shown in Figure 2.5b. The contact resistance follows Wexler's formula

$$R(T) = \frac{16\rho l}{3\pi d^2} + \beta\frac{\rho}{d}\,, \tag{2.6}$$

where β is a slowly varying function of l/d with values close to unity. This is approximately a sum of the ballistic Sharvin resistance and the thermal Maxwell's resistance [1, 2].

2.4 Eigenchannels and transmission coefficients

The diameter of small ballistic contacts usually lies in the range of a few nanometers. For much smaller contacts approaching the atomic limit, the concept of conduction channels is often applied. The contact is thought to consist of N individual channels, each channel i with a transmission coefficient τ_i that determines how large fraction of the current can pass, $0 \leq \tau_i \leq 1$, and i is an index running form 1 to N. The number of channels per constriction depends also on the structure of the valence orbitals of the atoms forming the contacts but can be roughly estimated to be

$$N \approx \left(\frac{k_F a}{2}\right)^2 , \tag{2.7}$$

where k_F is the Fermi wave number and a is the contact radius [27]. In this approach, the conductance of an atomic point contact can be obtained from the Landauer formula as a sum over all occupied channels

$$G = G_0 \sum_i \tau_i , \tag{2.8}$$

where $G_0 = 2e^2/h$ is the quantum conductance [1, 27].

2.5 Point-contact Andreev reflection spectroscopy

Because the superconductor has an energy gap in the density of single-electrons states where the electrons form Cooper pairs, the single electron current must be transformed to a Cooper pair current. In a simplified description, this means that when crossing the interface from the normal metal into the superconductor, the incident electron creates a pair and a corresponding hole is reflected back to the normal metal, as shown in Figure 2.6. Effectively two electrons are transported through the interface simultaneously. Because energy, momentum and spin must be conserved, the reflected hole and the created electron have properties closely related to those of the incident one. This process is known as Andreev reflection [30, 31], and it is described in more detail in Chapter 3.

Andreev reflection at superconductor - ferromagnet junctions is more complicated than in the case of non-magnetic normal conductor - superconductor contacts. This is

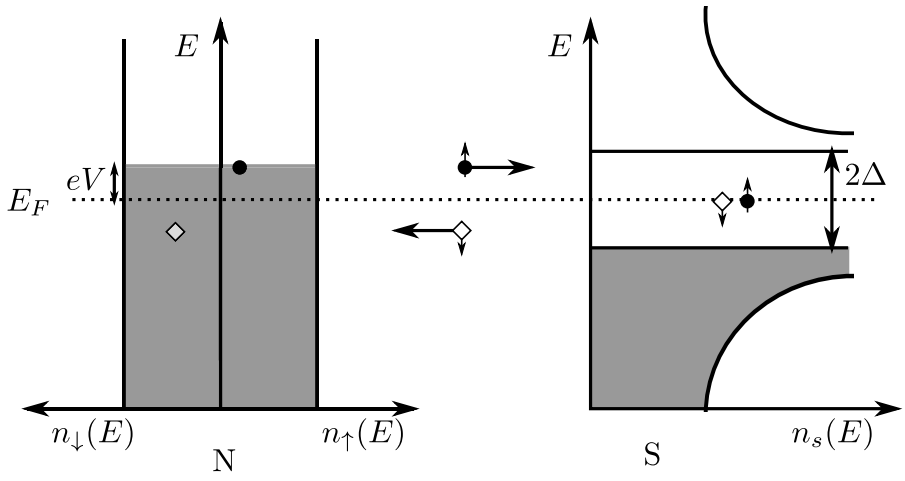

Figure 2.6: Andreev reflection at non-magnetic normal metal - superconductor interface. The incident electron (dot) from $+eV$ is reflected as a hole (empty diamond) at $-eV$. A Cooper pair is produced at the Fermi level in the superconductor.

because the Cooper pair consists of two electrons with opposite spins and therefore the reflected hole belongs to a different spin band than the original electron. If the normal metal is not spin polarized, there are equally many electrons of each spin species and therefore all electrons should be able to form a pair. In magnetically ordered materials on the other hand, a majority of electrons belong to one spin species and the minority to the other. Therefore only those majority spin electrons that are able to pair with a minority spin electron can cross the interface and participate in current transport. Thus for a ferromagnet only a part of the electrons can participate in current transport through Andreev reflection while the rest are reflected back from the interface [17].

In 1995 de Jong and Beenakker [17] suggested that Andreev reflection at superconductor - normal conductor point contacts could be used to detect the spin polarization. They pointed out that not all of the transmission channels can participate in Andreev reflection because the incident electron and the reflected hole belong to different spin bands. For a magnetically ordered material with an imbalance of spin up and down states this means that Andreev reflection can probe the magnitude of this imbalance. The first experimental results were obtained in 1998 by Soulen *et al.* [16] and Upadhyay *et al.* [32].

It was initially assumed that the polarization could be read off the zero bias resistance or conductance because when interface scattering is negligible, that is the strength

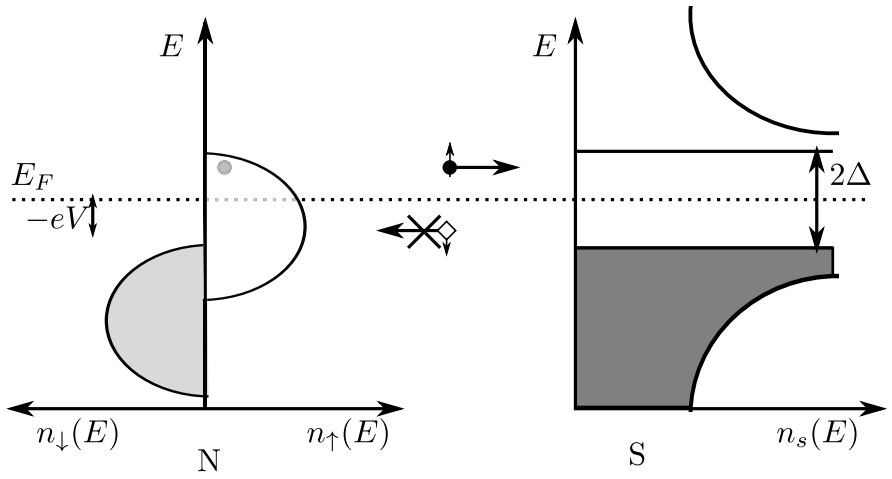

Figure 2.7: Andreev reflection is not possible at a half-metallic normal metal - superconductor interface. The incident electron (dot) from $+eV$ can not be reflected as a hole (empty diamond) at $-eV$ because there are no electron states in the corresponding spin band.

of the interface barrier $Z = 0$, the differential conductance of a point contact can be written in a form

$$\frac{1}{G_N}\frac{dI}{dV} = 2\,(1 - P_c)\ , \tag{2.9}$$

where G_N is the conductance in the normal state and P_c the spin polarization of the contact. This means that without an interface barrier and polarization the conductance would be doubled (resistance reduced to half of the normal state resistance) because of the two electrons effectively transported in the Andreev reflection process but in the polarized case this doubling is reduced by $(1 - P_c)$ [16]. In general, most contacts do not fulfil these assumptions but have some sort of interface barrier, possibly caused by an oxide layer or the mismatch of Fermi velocities at the interface [18] and these effects can lead to an overestimation of the polarization [33].

Spectra of superconductor - non-magnetic normal conductors have been analysed with a model by Blonder, Tinkham and Klapwijk [34], known as the BTK model, for more than 30 years. It is a one dimensional model that describes the interface with a δ function barrier with a strength Z. This model has been expanded to describe also the spin polarization of magnetically ordered metals [18, 35–37]. These models are presented in more detail in the next chapter. They have been applied to the measurement of spin polarization in a wide variety of materials in different forms ranging from bulk

materials [38–40] to thin films or foils [16, 18, 32, 39–42] and nanowires [43] as well as for a number of different metals from traditional ferromagnets [16, 18, 40] ferromagnetic alloys and compounds [38, 44–50] to Heusler alloys [51–54] and half-metal candidates including $La_{0.7}Sr_{0.3}MnO_3$ [39] and CrO_2 [55–57]. The measurements have been performed both as function of magnetic field [41] and temperature [38].

Despite the wide range of applications, point-contact Andreev reflection spectroscopy has also faced criticism. While the fabrication of point contacts can be very simple in comparison to other techniques, the analysis might not be as straightforward as it can seem and its validity has been questioned [36, 42, 58]. On a microscopic scale the exact experimental geometry is often unknown and unideal with deformations and imperfections. This can present itself as clearly visible additional features in the measured spectra [59] or subtly as more slight alterations from the ideal form. There have been many attempts to describe this situation theoretically. The BTK model has been expanded to the diffusive regime [35] and three dimensions [36, 60], and additional broadening parameters have been included [42, 61]. While in many cases the simple differential conductance or resistance curves can be uniquely described with this increasing set of parameters, this is not always the case and in general the increasing number of parameter tend to reduce this uniqueness [36, 58]. It is possible that several different physical phenomena have very similar effects on the spectra. It can, for example, be difficult to separate pair breaking effects from spin polarization, or to observe the suppression of the superconducting gap caused by local heating or the proximity of the ferromagnetic electrode when there is also scattering in the electrodes to cause broadening of the spectra [36].

	Photoemission [13]	Tunneling [15]	AR [16]	AR [18]
Fe	+54	+40±2	46±2	43± 0.03
Co	+21	+35±3	42±2	45±0.02
Ni	+15	+23±3	44±4	37±0.01

Table 2.1: Polarization values (%) measured with the three different techniques, spin polarized photoemission, spin polarized tunneling and Andreev reflection.

There are also questions related to the physical meaning of some of the fitting parameters in the BTK model as, for example, the origin of the Z parameter has been discussed [40, 42, 62]. Because δ functions only exist as approximations of reality, there have been attempts to understand the physical meaning of the Z parameter [40, 42, 62]. Blonder and Tinkham [62] argue that as the contacts are three dimensional the Z should be thought of as a phenomenological parameter related to the amount of elastic scattering at dislocations, other imperfections of the interface or an oxide layer at the contact. [42, 62] Blonder and Tinkham [62] also point out that the mismatch of the Fermi velocities v_F of the electrodes will cause some reflection in addition to the interface barrier and that this reflection is absorbed into the Z parameter. This will lead to Z having an effective value higher than that caused by the interface barrier alone

$$Z = \sqrt{Z_0^2 + \frac{|1 - r^2|}{4r}} \tag{2.10}$$

where r is the ratio of the Fermi velocities and Z_0 the contribution from the dielectric barrier. It is possible that this overestimates the effect of the mismatch because *ab initio* calculations have suggested that the contribution of this mismatch to Z should be smaller than those observed at point contacts [40, 63].

In addition, most point-contact Andreev reflection measurements of the spin polarization have found the polarization P to drop as function of the strength of the interface barrier Z. One possible reason for this drop has been suggested to be multiple scattering in the contact region so that the Z parameter would depend on both the average number of scattering events per electron d/l and the scattering anisotropy ψ according to

$$Z^2 = \frac{1}{1 + \psi} \frac{d}{l} \tag{2.11}$$

where d is the width of the scattering region, ψ a scattering anisotropy and l the electron mean free path [40]. Unfortunately these quantities are not directly measurable. Another explanation for this dependence could be that the polarization measured in point-contact spectroscopy is affected by the changing transport regime from ballistic to diffusive when the number of scattering events increases in the contact region [36, 42].

3. The Blonder-Tinkham-Klapwijk model

The BTK model by Blonder, Tinkham and Klapwijk [34] was aimed to fill the theoretical gap between the tunneling model and the description of metallic contacts by creating a model to describe arbitrary barrier strengths. It is a one-dimensional ballistic model and applies to non-magnetic normal metal-superconductor junctions. This chapter starts with a brief introduction to superconductivity and an overview of important concepts and continues then to describe the original BTK model and how it has been expanded to include the quasiparticle lifetime and the spin polarization.

3.1 Superconductivity

Superconductors can be defined as metals that in the absence of an external magnetic field lose all electrical resistance below a specific temperature called the critical temperature T_c. This means that in the superconducting state they do not have any electrical resistance. They are also perfect diamagnets that expel magnetic fields inside the superconductor when the field is not stronger than the critical magnetic field B_c. This second phenomenon is known as Meissner effect. Superconductivity can be destroyed both by increasing the temperature and the magnetic field. These transitions can be of first or second order [64].

Superconductors can be classified into type I and type II superconductors based on their transition from superconducting to normal state in an external magnetic field. For type I superconductors, the transition at the thermodynamical critical field H_c is of first order. For type II superconductors, the superconducting transition is of second order. These superconductors have two critical fields, H_{c1} and H_{c2}. At the lower critical field H_{c1} the magnetic field starts to penetrate into the superconductor in vortices that have a normal core while the rest of the material still remains superconducting. Only at the

upper critical field H_{c2}, the density of vortices becomes so large that the entire metal becomes normal conducting [65].

The single-electron density of states of a superconductor has a gap at the Fermi energy. This gap is called the energy gap and it is usually denoted as 2Δ. A schematic representation of the electronic density of states at the interface between a normal conductor and a superconductor is presented in Figure 3.1 [64].

Metals can be thought to consist of conduction electrons and a lattice of positive ions. Cooper showed in 1956 [66] that under attractive interaction of any strength a bound electron pair can form from the Fermi sea background. For conventional metals such an attractive interaction arises from the electron-phonon interaction of the conduction electrons and the positive ions of the lattice. Simplified, an electron moving through the lattice attracts the positive ions of the lattice towards its path. Because of their long relaxation time, these displaced ions will then attract a second electron which results in an attractive interaction between the two electrons. If this interaction is stronger than the repulsion from the screened Coulomb interaction, there will be a net attraction which leads to superconductivity [65]. These bound electron pairs are called Cooper pairs.

If one bound electron pair can form, it should also be possible that more of them will form. Bardeen, Cooper and Schrieffer [67] showed in 1957 that it is possible to have a ground state where all free electrons are bound to pairs that has a lower energy than the corresponding state of single electrons.

3.2 The BTK model

Flow of electric current across superconducting interfaces can be described with a semiconductor model where the superconducting density of states $N_s(E)$ is the only difference between the normal and superconducting states. The density of states of the normal conductor is assumed to be a continuous distribution of single particle states while the superconductor is described as a semiconductor with a gap 2Δ in the density of states as shown in Figure 3.1 [65]. The discussion in this section follows that of the paper by Blonder, Tinkham and Klapwijk [34].

In zero magnetic field, the interface between a superconductor and a normal conductor can be described with an appropriate set of boundary conditions and the Bogoliubov

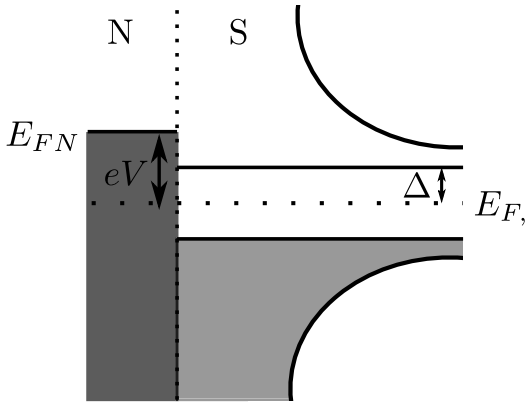

Figure 3.1: The density of states of a normal conductor (N) and a superconductor (S) in contact with each other. An applied bias voltage V shifts the Fermi energy of the normal conductor with respect to that of the superconductor.

equations

$$\begin{cases} i\hbar\dfrac{\partial f(x,t)}{\partial t} = \left(-\dfrac{\hbar^2\nabla^2}{2m} - \mu(x) + V(x)\right) f(x,t) + \Delta(x) g(x,t)\,, & (3.1) \\ i\hbar\dfrac{\partial g(x,t)}{\partial t} = -\left(-\dfrac{\hbar^2\nabla^2}{2m} - \mu(x) + V(x)\right) g(x,t) + \Delta^*(x) f(x,t)\,, & (3.2) \end{cases}$$

where $\Delta(x)$ is the superconducting pair potential, $\mu(x)$ the chemical potential and $V(x)$ a potential. The functions $f(x,t)$ and $g(x,t)$ are the wave functions of electrons and holes (time-reversed electrons). In the normal state the equations 3.1 and 3.2 become the Schrödinger equations for electrons and holes because there is no energy gap.

For clean materials and assuming a real and constant Δ in the superconductor, the Bogoliubov equations can be solved with plane-wave trial functions for the electron and hole

$$\begin{cases} f = \tilde{u} e^{i(kx - Et/\hbar)} & \text{and} \quad (3.3) \\ g = \tilde{v} e^{i(kx - Et/\hbar)}\,, & (3.4) \end{cases}$$

where $\tilde{u}$ and $\tilde{v}$ are numerical coefficients called coherence factors for which $\mid \tilde{u} \mid^2 + \mid \tilde{v} \mid^2 = 1$ holds, k is the momentum, x the position, t time and E the energy. When the external

potential $V(x)$ vanishes, the Bogoliubov equations 3.1 and 3.2 simplify to

$$\begin{cases} E\tilde{u} = \left[\dfrac{\hbar^2 k^2}{2m} - \mu\right]\tilde{u} + \Delta\tilde{v} & (3.5) \\ E\tilde{v} = -\left[\dfrac{\hbar^2 k^2}{2m} - \mu\right]\tilde{v} + \Delta\tilde{u}\,. & (3.6) \end{cases}$$

Energies E that satisfies this equation pair are

$$E^2 = \left(\frac{\hbar^2 k^2}{2m} - \mu\right)^2 + \Delta^2\,, \tag{3.7}$$

which has positive and negative roots. This solution leads to the following equations for the coherence factors and momentum

$$\tilde{u}^2 = \frac{1}{2}\left[1 \pm \frac{\sqrt{E^2 - \Delta^2}}{E}\right] = 1 - \tilde{v}^2 \tag{3.8}$$

$$\hbar k^{\pm} = \sqrt{2m}\sqrt{\mu \pm \sqrt{E^2 - \Delta^2}}\,. \tag{3.9}$$

For energies $E \geq 0$, it can be defined that

$$u_0^2 = 1 - v_0^2 = \frac{1}{2}\left(1 + \frac{\sqrt{E^2 - \Delta^2}}{E}\right)\,. \tag{3.10}$$

In the BTK model, the scattering at the interface is modelled with a δ-function potential

$$V(x) = H\delta(x)\,. \tag{3.11}$$

The potential has a dimensionless strength

$$Z = \frac{mH}{\hbar^2 k_F} = \frac{H}{\hbar v_F}\,, \tag{3.12}$$

where k_F is the Fermi wave number and v_F the Fermi velocity.

The states allowed for electrons at an interface are drawn in Figure 3.2. In equilibrium they all are equally probable. There are four different possible transmission and reflection processes for an incident electron above the superconducting energy gap Δ at position 0 in Figure 3.2. It can be Andreev reflected to a hole at position 6 with probability $A(E)$, normal reflected to position 5 with probability $B(E)$, transmitted either with wave vector on the same side of the Fermi surface to 4 with probability $C(E)$ or with wave vector on the other side of the Fermi surface to 2 with probability $D(E)$. Inside the energy gap the last two transmission processes are forbidden. The sum of the probabilities must always be conserved and therefore must fulfil

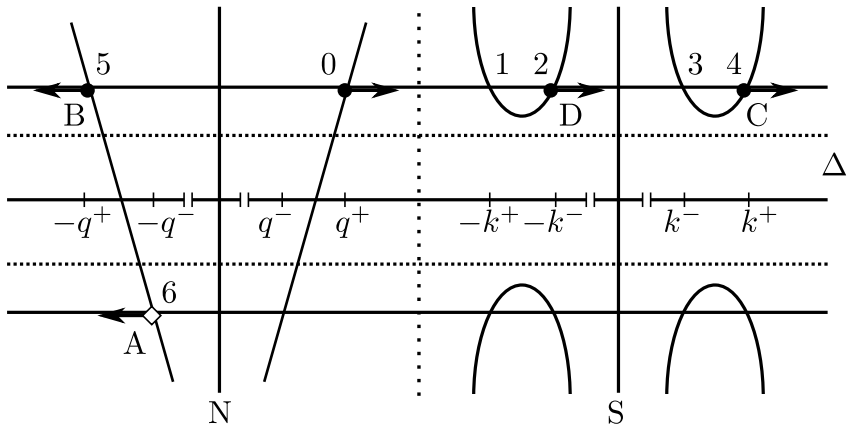

Figure 3.2: Energy versus momentum at a superconductor - normal conductor interface according to [34].

$A(E) + B(E) + C(E) + D(E) = 1$. They can be calculated from the solutions of the Bogoliubov equations.

If the incident electron produces only outgoing particles, the wave functions at the interface are

$$\psi_{inc} = \begin{pmatrix} 1 \\ 0 \end{pmatrix} e^{iq^+ x}\,, \tag{3.13}$$

$$\psi_{refl} = a\begin{pmatrix} 0 \\ 1 \end{pmatrix} e^{iq^- x} + b\begin{pmatrix} 1 \\ 0 \end{pmatrix} e^{-iq^+ x}\,, \tag{3.14}$$

$$\psi_{trans} = c\begin{pmatrix} u_0 \\ v_0 \end{pmatrix} e^{ik^+ x} + d\begin{pmatrix} v_0 \\ u_0 \end{pmatrix} e^{-ik^- x}\,, \tag{3.15}$$

where $\hbar q^\pm = \sqrt{2m}\sqrt{\mu \pm E}$ and the notation

$$\psi = \begin{pmatrix} f(x) \\ g(x) \end{pmatrix} \tag{3.16}$$

is used. The constants a, b, c and d can be calculated using boundary conditions that require that the wave function is continuous at the interface and that its derivative fulfils

$$\frac{\hbar}{2m}\left(\frac{\partial \psi_S}{\partial x} - \frac{\partial \psi_N}{\partial x}\right) = H\psi(0)\,, \tag{3.17}$$

when the interface barrier is $V(x) = H\delta(x)$. It has also been assumed that $q^- = q^+ =$

$k^- = k^+ = k_F$. The coefficients become

$$a = \frac{u_0 v_0}{\gamma} \tag{3.18}$$

$$b = -\frac{(u_o^2 - v_0^2)(Z^2 + iZ)}{\gamma} \tag{3.19}$$

$$c = \frac{u_0(1 - iZ)}{\gamma} \tag{3.20}$$

$$d = \frac{iv_0 Z}{\gamma}\,, \tag{3.21}$$

where $\gamma = u_0^2 + (u_0^2 - v_0^2)Z^2$. These coefficients are related to the probabilities of the transmission and reflection processes at the interface. The probability of Andreev reflection $A = a^* a$ where a^* is the complex conjugate of a, the probability of normal reflection $B = b^* b$ and the transmission probabilities are $C = c^* c(u_0^2 - v_0^2)$ and $D = d^* d(u_0^2 - v_0^2)$. They are listed in Table 3.1.

Current over a voltage biased junction can in general be calculated by solving the Boltzmann equation. The situation is more simple in the ballistic regime where scattering in the contact region can be ignored. The distribution functions of incoming particles can be described with Fermi-Dirac functions at equilibrium shifted in energy. The incoming electrons from the normal metal have a distribution $f_0(E - eV)$ and those from the superconductor $f_0(E)$.

For simplicity, the current I is calculated on the normal side of the contact where there is no supercurrent. It becomes

$$I = 2N(0) e v_F \mathcal{A} \int_{-\infty}^{\infty} \left(f_{\rightarrow}(E) - f_{\leftarrow}(E)\right) dE\,, \tag{3.22}$$

where $\mathcal{A}$ is an effective area of the contact, $N(0)$ is the density of states at Fermi energy E_F and the arrows point to the direction of the particles momenta. The distributions are

$$f_{\rightarrow}(E) = f_0(E - eV) \quad \text{and} \tag{3.23}$$

$$f_{\leftarrow}(E) = A(E)\left(1 - f_{\rightarrow}(E)\right) + B(E) f_{\rightarrow}(E) + \left(C(E) + D(E)\right) f_0(E)\,, \tag{3.24}$$

where A, B, C and D are the probabilities of reflection and transmission processes listed in Table 3.1. The current can now be written as

$$I = 2N(0) e v_F \mathcal{A} \int_{-\infty}^{\infty} \left(f_0(E - eV) - f_0(E)\right)\left(1 + A(E) - B(E)\right) dE\,. \tag{3.25}$$

		A	B	C	D
Normal state		0	$\frac{Z^2}{1+Z^2}$	$\frac{1}{1+Z^2}$	0
Superconducting state					
	$E < \Delta$	$\frac{\Delta^2}{E^2+(\Delta^2-E^2)(1+2Z^2)^2}$	$1-A$	0	0
	$E > \Delta$	$\frac{u_0^2 v_0^2}{\gamma^2}$	$\frac{(u_0^2-v_0^2)^2 Z^2(1+Z^2)}{\gamma^2}$	$\frac{u_0^2(u_0^2-v_0^2)^2(1+Z^2)}{\gamma^2}$	$\frac{v_0^2(u_0^2-v_0^2)^2 Z^2}{\gamma^2}$

Table 3.1: The probabilities of reflection and transmission processes at superconductor - normal conductor interfaces [34].

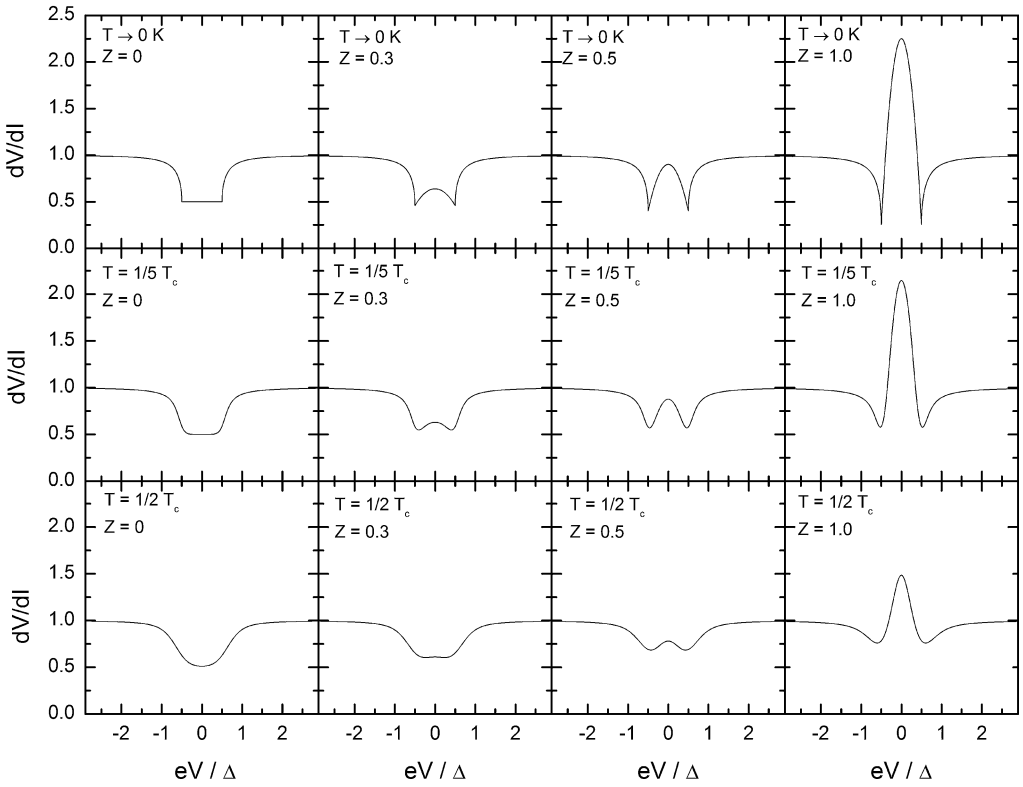

Figure 3.3: Spectra created with the BTK model with varying temperature and Z parameter. The temperature dependence of the energy gap follows the BCS relation $2\Delta(T=0)/kT_c = 3.53$.

Finite temperatures are included through the Fermi-Dirac distribution. This equation could be integrated numerically to obtain the current as function of voltage, but it is often easier to directly calculate its derivative dV/dI. Examples of differential resistance spectra created using this model are in Figure 3.3 [34].

3.3 Finite quasiparticle lifetime in the BTK model

Occasionally the measured differential resistance or conductance spectra of superconductor - normal conductor contacts have been broader than predicted by the BTK model. There have been a number of ways to explain these deviations ranging from additional thermal broadening [40, 48, 58] to a spreading resistance of thin films [47]. Another option is to describe the broadening with a finite quasiparticle lifetime τ caused by inelastic electron-electron scattering. It was first introduced for tunneling contacts [68, 69]

and has later been applied also for direct contacts [61, 70, 71]. In this approach the density of states is affected by the broadening. The broadening parameter $\Gamma = \hbar/\tau$ alters the energy with $E - i\Gamma$ [68, 69, 71] or with $E + i\Gamma$ [61]. Following the notation by de Wilde *et al.* [71], this can be included into the BTK model by adding an inelastic scattering term to the trial plane wave functions $f(x,t)$ and $g(x,t)$

$$f(x,t) = \tilde{u}e^{ikx - i(E - i\Gamma)t/\hbar} \quad \text{and} \tag{3.26}$$

$$g(x,t) = \tilde{v}e^{ikx - i(E - i\Gamma)t/\hbar}\,. \tag{3.27}$$

Like before when the external potential $V = 0$, the Bogoliubov equations 3.1 and 3.2 simplify to

$$\begin{cases} (E - i\Gamma)\,\tilde{u} = \left[\dfrac{\hbar^2 k^2}{2m} - \mu\right]\tilde{u} + \Delta\tilde{v} & (3.28) \\ (E - i\Gamma)\,\tilde{v} = -\left[\dfrac{\hbar^2 k^2}{2m} - \mu\right]\tilde{v} + \Delta\tilde{u} & (3.29) \end{cases}$$

after the derivations. They lead to two solutions for the energy

$$(E - i\Gamma)^2 = \left[\frac{\hbar^2 k^2}{2m} - \mu\right]^2 + \Delta^2\,. \tag{3.30}$$

The positive solution corresponds to the coherence factors

$$u_0^2 = \frac{1}{2}\left[1 + \frac{\sqrt{(E - i\Gamma)^2 - \Delta^2}}{E - i\Gamma}\right] = 1 - v_0^2\,. \tag{3.31}$$

These coherence factors are no longer complex conjugates of each other.

In the BTK model the density of quasiparticle states is

$$N_S = \mathrm{Re}\left[(u_0^2 - v_0^2)^{-1}\right]\,. \tag{3.32}$$

When inelastic scattering is included this becomes

$$N_S = \mathrm{Re}\left[\frac{E - i\Gamma}{\sqrt{(E - i\Gamma)^2 - \Delta^2}}\right]\,. \tag{3.33}$$

This means that unlike many of the other broadening mechanisms, the inelastic scattering affects directly the density of states.

The boundary conditions and the solution for the coefficients a and b do not change. The probabilities for Andreev and normal reflection have the same form as for the BTK model without lifetime broadening but the coherence factors u_0 and v_0 have changed. Examples of spectra created with the BTK model that includes the lifetime parameter Γ are presented in Figure 3.4.

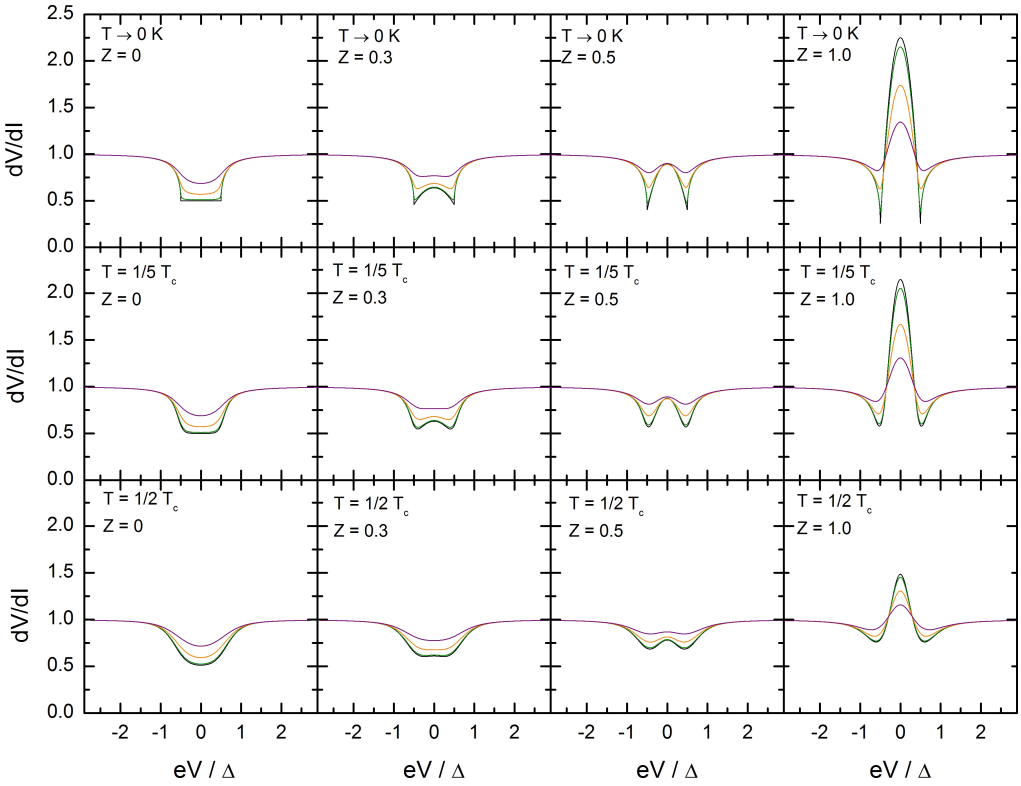

Figure 3.4: Examples of spectra of the BTK model modified to include the finite lifetime of quasiparticles. The values of the lifetime parameter Γ were 1 % (green line), 7 % (orange line) and 20 % (purple line) of the energy gap $2\Delta(T = 0\mathrm{K})$. The black line shows the spectra without lifetime broadening. The temperature dependence of the energy gap follows the BCS relation $2\Delta(T = 0\mathrm{K})/kT_c = 3.53$.

3.4 Spin polarization in the BTK model

Possibly the simplest and most natural way to define the spin polarization is to use the density of states at the Fermi level for each spin to define the spin polarization,

$$P = \frac{N_\uparrow - N_\downarrow}{N_\uparrow + N_\downarrow} \,. \tag{3.34}$$

This polarization can be accessed with spin polarized photoemission [11] and tunnel junctions [15].

Strijkers's model

A second definition more suited for the point-contact measurements is obtained when one discusses current transport which is not only related to the density of states. The current I can be divided into two currents, $I_\uparrow$ and $I_\downarrow$ according to the spin of the electrons as

$$I = I_\uparrow + I_\downarrow = (1 - P)I_u + PI_p \,, \tag{3.35}$$

where I_u and I_p are the currents in the fully unpolarized ($P = 0$) and polarized ($P = 1$) case, respectively. The unpolarized portion of the current $(1 - P)I_u$ can take part in Andreev reflection while the polarized current PI_p can not be Andreev reflected. This leads to a polarization of

$$P = \frac{I_\uparrow - I_\downarrow}{I_\uparrow + I_\downarrow} = \frac{N_\uparrow v_{F,\uparrow} - N_\downarrow v_{F,\downarrow}}{N_\uparrow v_{F,\uparrow} + N_\downarrow v_{F,\downarrow}} \,, \tag{3.36}$$

where $N_\uparrow$ and $N_\downarrow$ are again the densities of states at Fermi level and $v_{F,\uparrow}$ and $v_{F,\downarrow}$ the Fermi velocities of each of the spin species [11, 16, 18].

Strijkers *et al.* [18] have used this definition as a base for their model that expands the BTK model to magnetic metals. When the superconducting pair potential is a constant, the probabilities $A(E)$ and $B(E)$ for Andreev reflection and normal reflection can again be calculated from solutions of the Bogoliubov equations with plane wave trial functions separately for the polarized and unpolarized parts of the current. The boundary conditions stay the same for both currents and for the unpolarized part the solution is exactly the same as in the original BTK model. It is assumed that the probability for Andreev reflection vanishes for the polarized current. The probabilities for Andreev and normal reflection are tabulated in Table 3.2. With the probabilities the current through the contact as function of bias voltage can be solved using equation 3.25. Examples of spectra calculated with this model are shown in Figure 3.5.

	Unpolarized current		Polarized current	
	A_u	B_u	A_p	B_p
$\lvert E\rvert \leq \Delta$	$\dfrac{\Delta^2}{E^2+(\Delta^2-E^2)(1+2Z^2)^2}$	$1-A_u$	0	1
$\lvert E\rvert \geq \Delta$	$\dfrac{u_0^2 v_0^2}{\gamma^2}$	$\dfrac{(u_0^2-v_0^2)^2 Z^2(1+Z^2)}{\gamma^2}$	0	$\dfrac{(u_0^2-v_0^2)^2 Z^2(1+Z^2)}{\gamma^2-u_0^2 v_0^2}$

Table 3.2: The probabilities for Andreev reflection A and normal reflection B for both fully unpolarized and polarized currents in the Strijkers' model. The notation $u_0^2 = 1-v_0^2 = \frac{1}{2}\left(1+\sqrt{(E^2-\Delta^2)/E^2}\right)$ and $\gamma^2 = u_0^2 v_0^2 + (u_0^2-v_0^2)\left[u_0^2+Z^2+(u_0^2-v_0^2)Z^2(1+Z^2)\right]$ is used [18].

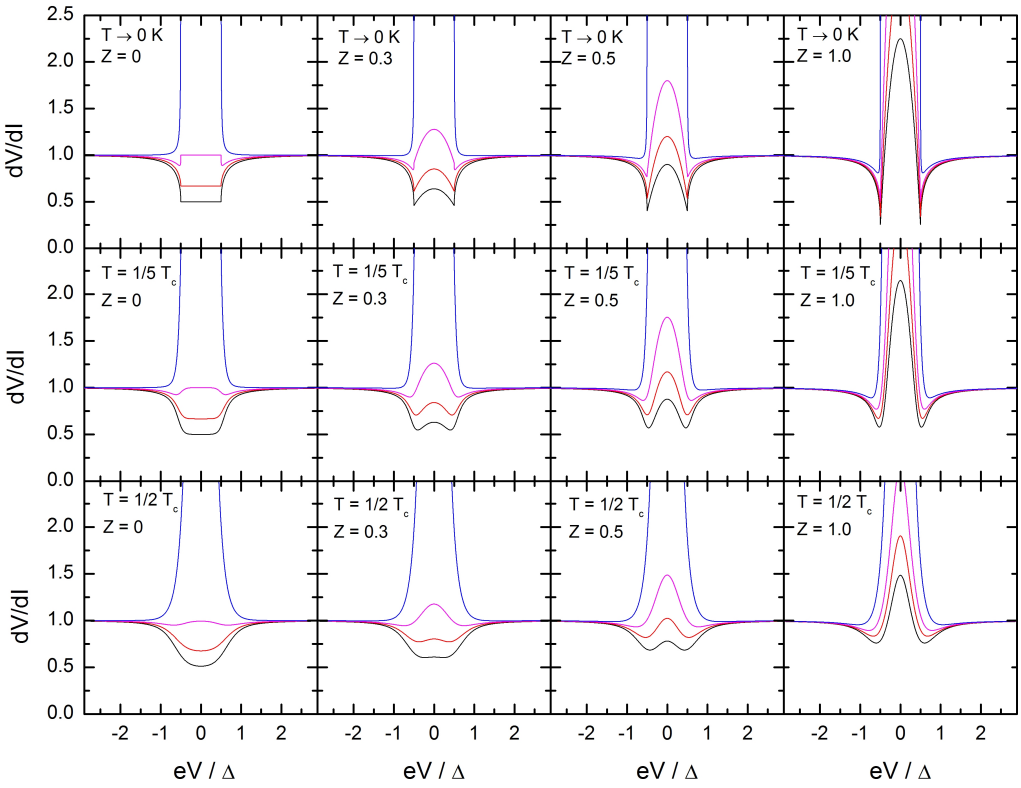

Figure 3.5: Spectra of the BTK model modified to include the spin polarization [18] with various parameter values. The temperature dependence of the energy gap follows the BCS relation $2\Delta(T=0)/kT_c = 3.53$. The polarization has values $P = 0$ (black curve), $P = 0.25$ (red), $P = 0.5$ (pink) and $P = 1.0$ (blue). For $P = 1.0$ at the lowest temperatures the differential resistance is not defined inside the energy gap and at higher temperatures it has a finite but large value.

Mazin's model

Mazin *et al.* [35] use the scattering approach of independent conduction channels for each spin to calculate the spectra of superconductor-ferromagnet contacts. In the polarized case the number of channels for the spins can be different from each other. Its main difference when compared to the Strijkers model is the treatment of the probability of Andreev reflection above the superconducting energy gap. The plane wave reflected from the interface becomes a combination of a plane wave and an evanescent wave. This means that the Andreev reflection probability is non-zero above the energy gap even though the evanescent wave does not carry current but this does enhance the transparency of the interface. The resulting conductances are tabulated in table 3.3 with the ones from the Strijkers model as reference [35]. The final value for the spin polarization has been shown to be nearly independent of the choice of the model [33, 36].

Pérez-Willard

In this model the current is divided into two spin currents $I = I_\uparrow + I_\downarrow$ that both have their own transmission coefficients $\tau_\uparrow$ and $\tau_\downarrow$ while in most other modifications of the BTK model the transmission coefficient is assumed to be the same for electrons of both spin directions. The spin polarization is defined by these two transmission coefficients

$$P = \frac{|\tau_\uparrow - \tau_\downarrow|}{\tau_\uparrow + \tau_\downarrow} \,. \tag{3.37}$$

Pérez-Willard *et al.* [37] use Greens functions to describe the interface and a normal state scattering matrix to set the boundary conditions. The current is calculated with equation 3.25 like in the original BTK model but the probabilities A and B for Andreev and normal reflection originate from the scattering matrix. The equations for the conductance of a superconductor - ferromagnet interface are tabulated in Table 3.3 [37]. It has been reported that the polarization values extracted from the measured spectra with this model are larger than those from the Strijkers model [18] but an exact comparison is again difficult because there is no direct relation between the parameters of the two models [37].

Chalsani's 3D model

This model includes three dimensional spin dependent transmission and reflection probabilities $T_{\uparrow(\downarrow)}$ and $R_{\uparrow(\downarrow)}$ with $T_{\uparrow(\downarrow)} + R_{\uparrow(\downarrow)} = 1$. The transmission through an interface

	$E < \Delta$	$E > \Delta$
Unpolarized	$\frac{2(1+\beta^2)}{\beta^2+(2+2Z^2)^2}$	$\frac{2\beta}{1+\beta+2Z^2}$
Fully polarized (Strijkers)	0	$\frac{1+\beta(1+2Z^2)}{(1+\beta)(1+2Z^2)+2Z^4}$
Fully polarized (Mazin)	0	$\frac{4\beta}{(1+\beta)^2+4Z^2}$
Pérez-Willard	$\frac{4e^2}{h}\frac{\tau_\uparrow\tau_\downarrow}{(1+r_\uparrow r_\downarrow)^2-4r_\uparrow r_\downarrow(ev/\Delta)^2}$	$\frac{4e^2}{h}\frac{\tau_\uparrow\tau_\downarrow+(\tau_\uparrow+\tau_\downarrow-\tau_\uparrow\tau_\downarrow)\sqrt{1-(\Delta/eV)^2}}{\left[(1-r_\uparrow r_\downarrow)-(1+r_\uparrow r_\downarrow)\sqrt{1-(\Delta/eV)^2}\right]^2}$

Table 3.3: The conductance as function of bias voltage at zero temperature of the BTK model modified to take into account the spin polarization of the normal electrode for the Strijkers' and Mazin's models [33] and the Pérez-Willard model [37].

depends on the angle θ at which the incident electrons approach the interface. Therefore average transmission coefficients $\overline{T}_{\uparrow,\downarrow}$ for each of the spin species are calculated by averaging over all incident angles from $-\pi/2$ to $\pi/2$ with respect to the normal of the interface. This leads to a total conductance of

$$G = N_{\uparrow}\overline{T}_{\uparrow} + N_{\downarrow}\overline{T}_{\downarrow}\,. \tag{3.38}$$

The polarization of the current transmitted through the interface,

$$P_T = \frac{G_{\uparrow} - G_{\downarrow}}{G_{\uparrow} + G_{\downarrow}} = \frac{N_{\uparrow}\overline{T}_{\uparrow} - N_{\downarrow}\overline{T}_{\downarrow}}{N_{\uparrow}\overline{T}_{\uparrow} + N_{\downarrow}\overline{T}_{\downarrow}}\,, \tag{3.39}$$

is in many cases not the same as the polarization P defined using the densities of states at the Fermi level in equation 3.34 because $\overline{T}_{\uparrow}$ and $\overline{T}_{\downarrow}$ are not necessarily equal [36].

3.5 Fitting with multiple parameters

With two or three adjustable parameters the fitting is rather straightforward, because the fit quality can easily be evaluated. With more parameters the changes in the fit quality can be rather small and there can be multiple sets of fit parameters that describe the spectra equally well [36, 58]. Woods *et al.* attempted to limit the number of parameters by fixing the superconducting energy gap 2Δ [42] to its BCS value obtained from the critical temperature of the contact. Bugoslavsky *et al.* [58] suggested to minimize the variance between fit and measured spectrum to separate the degenerate solutions from each other. The variance between the normalized measured spectrum ($S_{meas} = (1/R_N)dV/dI(V)$) and fit ($S_{fit}(V)$) over the measured voltages V_i is defined as

$$\chi^2 = \frac{1}{N}\sum_{i}^{N}(S_{meas}(V_i) - S_{fit}(V_i))^2\,. \tag{3.40}$$

4. Experimental details

We have investigated point contacts between superconductors and normal conducting metals. The contacts were fabricated with the shear method by crossing two macroscopic wires with diameters of either 0.25 mm or 0.5 mm. Using the shear method allowed the diameter of the contact to be varied *in situ* but kept the contacts still rather stable during thermal cycling. The superconductors were Nb, Ta, Sn, Al and Zn, and the ferromagnetic metals Co, Fe and Ni. The non-magnetic normal conductors Ag, Au, Cu, Pd and Pt were used as reference, though not all possible combinations were measured. The properties of the superconductors are listed in Table 4.1. Often the surfaces of the samples were first cleaned with fine abrasive paper and then with ultrasound in an ethanol bath. Dilute HCl acid treatment was sometimes used to remove the oxide layer of Zn (one out of two samples) and Al (two out of twelve samples). It is generally assumed that the brushing motion of the wires against each other before the contact is formed breaks the possible oxide barriers at the contact interface. The measurements were performed either at 4.2 K in liquid He or at varying temperatures from below 0.1 K up to 10 K in vacuum in a dilution refrigerator.

For measurements at 4.2 K the sample stage of Figure 4.1a is connected to a dipstick and immersed in liquid He. For that the two sample wires are (Cu-coated if necessary) soldered to the sample holder (Figure 4.1b). One of the wires is connected to a movable rod that can be used to change the position and size of the contact.

The measurements at varying temperatures are performed in a dilution refrigerator which can be cooled down to below 0.1 K. The sample stage (Figure 4.2a) sits in vacuum and is connected to the mixing chamber of the cryostat. The setup for fabricating the contacts is shown in Figure 4.2b. The wires are connected to the Cu pieces that are glued electrically insulated on top of a bending plate. When the plate is bent, the wires move towards each other, changing both the position and the size of the contact.

The differential resistance dV/dI can be measured with a modulation technique where the dc current I running through the contact is modulated with a small ac com-

	T_c (K)	$B_c(T = 0\text{K})$ (mT)	$2\Delta(T = 0\text{K})$ (meV)
Nb	9.2	198	3.0
Ta	4.3	83	1.3
Sn	3.7	30.5	1.1
Al	1.2	9.9	0.35
Zn	0.88	5.3	0.24

Table 4.1: Critical temperatures, fields and energy gaps (at $T = 0$ K) of the traditional low temperature superconductors used in our measurements [64].

ponent $\tilde{I}$ at frequency f. When this component is sufficiently small, the corresponding dc voltage can be obtained as the first term of a Taylor expansion

$$V\left(I + \tilde{I}\cos(ft)\right) = V(I) + \frac{dV}{dI}\tilde{I}\cos(ft) + \frac{1}{2}\frac{d^2V}{dI^2}\tilde{I}\cos^2(ft) + \cdots . \qquad (4.1)$$

The differential resistance dV/dI can be obtained by measuring the ac voltage dV at frequency f.

The schematics of the electronic circuit used in our measurements are shown in Figure 4.3. The computer produces the dc part and the oscillator the ac part (frequency $f = 372$ Hz) of the excitation voltage. They are fed through two galvanometric decouplers to break ground loops and two series resistors to generate the dc and the ac currents. The resistors vary from 100 Ω to 10 MΩ for the dc current and are 100 times larger for the ac current (except for the largest resistance which is 100 MΩ). The current is fed into the cryostat, through the point contact and back to ground potential outside of the cryostat. The series resistors define the currents rather precisely, and they are always chosen to be much larger than the contact resistance. The absolute error in the dc current caused by the resistance of the contact is smaller than 1 percent.

The voltage drop across the contact is measured separately. The signal from the sample is first amplified with the voltage preamplifier (DL instruments, Model 1201). Then the ac voltage drop over the contact is measured with a lock-in amplifier at a frequency $f = 372$ Hz of the ac modulation. The dc voltage drop is recorded with

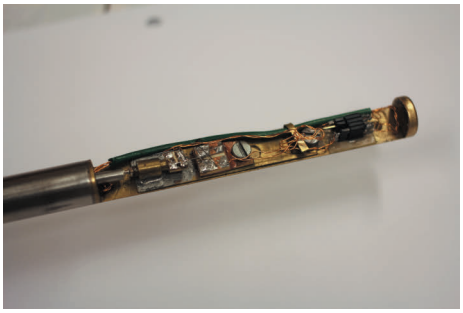

(a) Sample stage at 4.2 K.

(b) Set up at 4.2 K.

Figure 4.1: The experimental setup for fabricating shear method point contacts in liquid He at 4.2 K. a) The entire sample stage that is immersed in liquid He. b) The setup for fabricating shear contacts in liquid He where one can see the two silvery-looking wires almost forming a cross. The point-contact is formed at the intersection of the wires.

the analogue-digital converter ADC at the computer to obtain the differential-resistance spectrum of the contact. The signal can also be viewed with an oscilloscope.

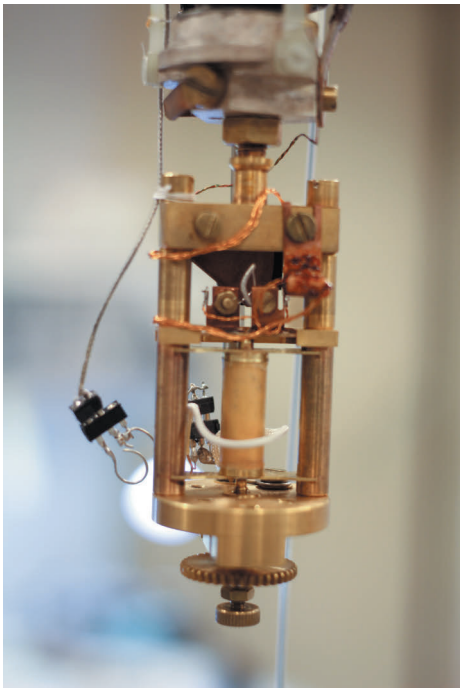

(a) Sample stage of the dilution refrigerator.

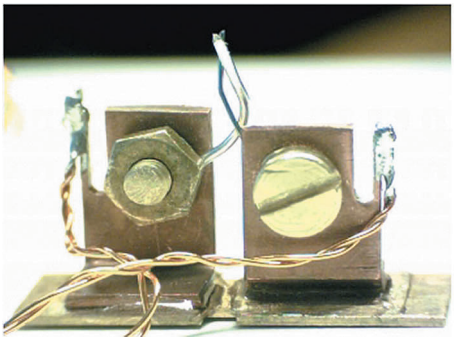

(b) Sample holder of the dilution refrigerator.

Figure 4.2: The experimental setup for fabricating shear method point contacts in vacuum. a) The sample stage for fabricating point contacts with the shear method attached to the mixing chamber of the dilution refrigerator. The mixing chamber is the grey part on top of the figure. The sample wires on the bending plate are in the centre of the figure, above the yellow vertical rod which is a piezo tube used as pushing rod to bend the bending plate. b) The sample holder for the wires forming the shear contacts. The sample wires are attached to Cu pieces with screws. The current and voltage leads are soldered to the Cu pieces that are glued electrically insulated onto a bending plate.

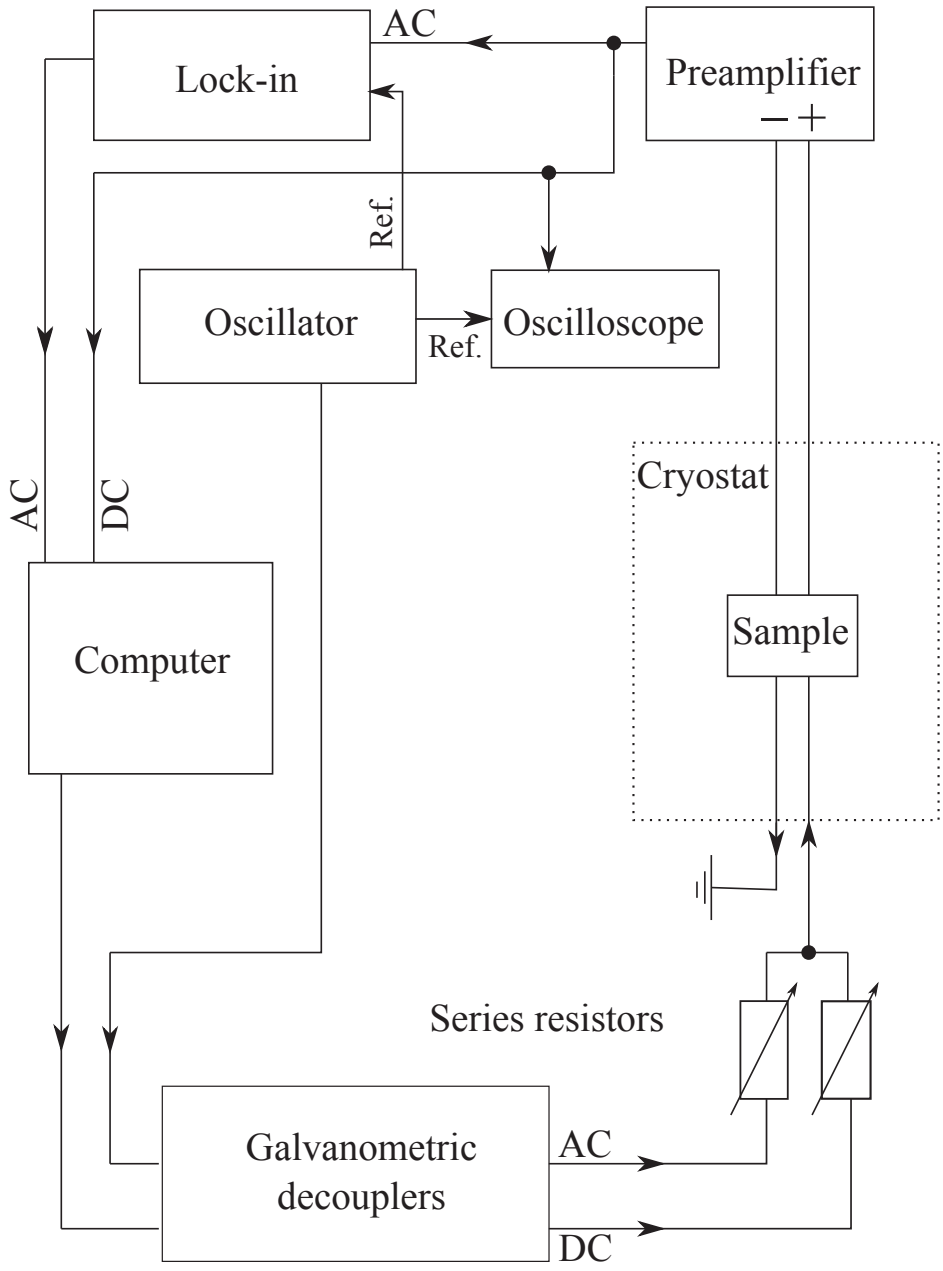

Figure 4.3: A schematic view of the electronic system used to measure differential resistance point-contact spectra.

5. Polarization measurements at 4.2 K

5.1 Andreev-reflection spectroscopy of ferromagnets: the impact of Fermi surface mismatch [P1]

In order to measure the spin polarization of a ferromagnetic sample we measured differential resistance spectra of point contacts between superconducting Nb ($T_c = 9.2$ K) and ferromagnet Co at 4.2 K in liquid He. Contacts with non-magnetic Cu were measured as a reference. [**P1**]

With the Strijkers' polarization model [18] we found that the spectra of Co in contact with superconducting Nb could be fitted with a polarization value that agrees well with those presented in the literature [16, 18, 40, 50, 59]. We also found that the spectra of Cu can be fitted with the lifetime model without polarization. However, it turned out that also the spectra of non-magnetic Cu could equally well be fitted with the polarization model and a non-zero spin polarization P, and the spectra of ferromagnetic Co with a zero spin polarization and a finite lifetime parameter Γ in the lifetime model. Examples of these fits are shown in Figure 5.1. This agrees with the results obtained for Pb-Pt-Cu and Pb-Pt-Co contacts of Chalsani *et al.*[36] measured at 4.2 K and 1.5 K. [**P1**]

We also found that when the polarization P is small but the Z parameter large, the two models can not be separated from each other but when the polarization increases and Z decreases, the fitting quality deteriorates. At intermediate values differences appear at the shoulders of the spectra and at ideal interfaces with $Z = 0$ the lifetime model produces a much broader spectrum. This is shown in Figure 5.2 where the theoretical curves from the polarization model were fitted with the lifetime model. This was also visible when fitting the measured spectra but the model that gave the best fit varied. [**P1**]

The magnitudes of the polarization P or the lifetime parameter Γ did not vary sig-

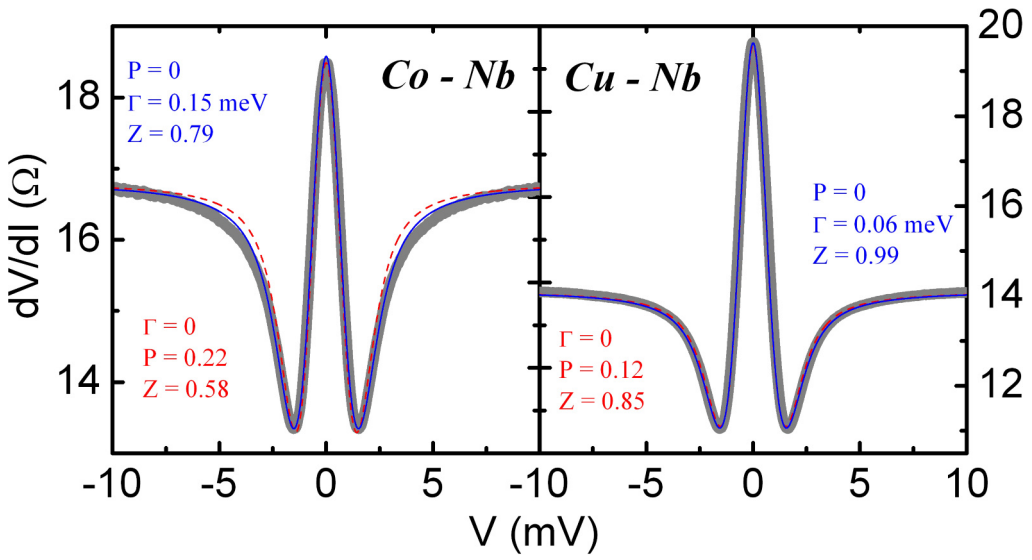

Figure 5.1: Measured differential resistance versus bias voltage (thick grey solid lines) together with fits with the Strijkers' polarization model ($\Gamma = 0$, red dashed lines) and the lifetime model ($P = 0$, blue solid lines). Deviations between fits and the measured spectra are found only near the shoulder where double minimum turns into the horizontal normal-state spectrum. The contact resistance $R_N(V)$ was taken to be a constant because no data above T_c was not available. (a) Nb - Co at T = 4.2 K and $2\Delta = 2.6$ meV, (b) Nb - Cu at T = 4.2 K and $2\Delta = 2.5$ meV. [**P1**]

nificantly between the ferromagnetic and the non-magnetic metals (Figure 5.3). We also observed a dependence $P(Z)$ similar to earlier studies [18, 40] for both material combinations, and found no difference between the $P(Z)$ dependencies of the ferromagnet and the non-magnet. The lifetime parameter Γ seemed to be independent of Z for these two metal combinations. Re-analysis of earlier $AuIn_2$ - Cu contacts data from [72] produced similar results. [**P1**]

5.2 Spin polarization versus lifetime effects at point contacts between superconducting niobium and normal metals [P2]

We expanded the measurements to contacts between superconducting Nb and ferromagnetic Fe and Ni, as well as non-magnetic Ag and Pt as reference. The results agreed with our previous data for Nb - Co and Nb - Cu contacts. The fit quality was good for ferromagnets and non-magnets with both models (Figure 5.4), and also their Z de-

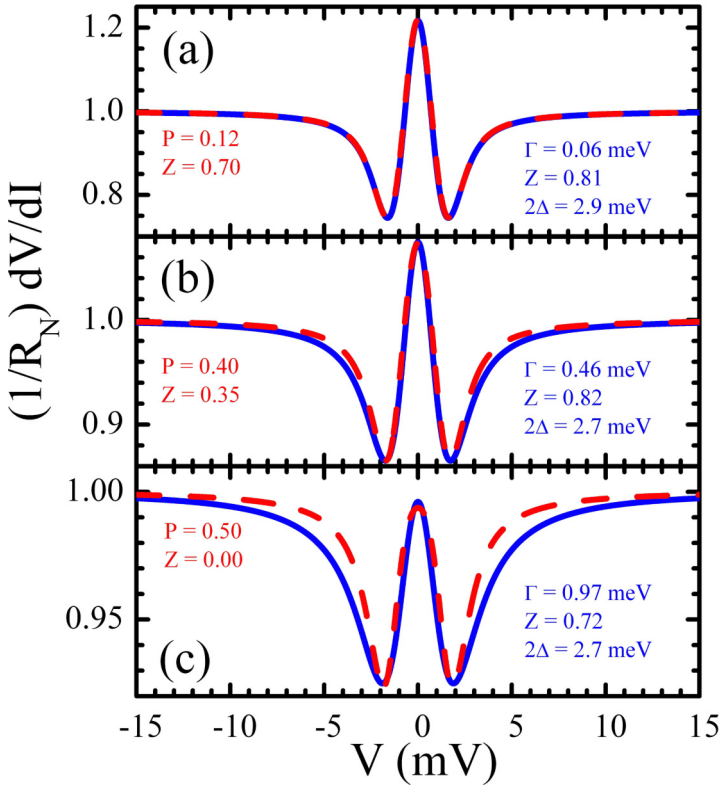

Figure 5.2: Normalized theoretical spectra from the Strijkers' polarization model (red dashed lines) fitted with the lifetime model (blue solid lines). The parameters of the polarization model indicated in the figures were chosen to match those from the analysis of the measured spectra. The energy gap was $2\Delta(T = 0) = 3.0$ meV and the temperature $T = 4.2$ K. [**P1**]

pendencies of the spin polarization as well as the extrapolated polarization values are indistinguishable (Figure 5.5).

5.3 Discussion

Without the knowledge that the non-magnetic metals should have a spin polarization equal to zero, applying the spin-polarized model blindly to our data would imply that Ag, Cu and Pt are polarized with a spin polarization close to 0.5. It would be equally possible to mistake the ferromagnets as unpolarized. It is clear that these two different descriptions of the experimental spectra can not be correct simultaneously. This difference should be measurable.

It is difficult to justify choosing one model to use for metals that are assumed to be ferromagnets and an other one for those that are assumed to be non-magnetic. This might be reasonable for well-known materials like the ones we have been investigating but if point-contact Andreev reflection spectroscopy is to be used to determine the spin polarization of new or unknown materials, it has to be able to separate non-magnetic metals from magnetically ordered ones. This would require the solutions of the modified BTK models to be unique and non-degenerate, or alternatively a separate method for determining which of them should be applied to the situation in question.

In order to separate non-magnetic materials from magnetically ordered ones, additional information is needed. One possibility would be to attempt to fix some of the fit parameters in order to use both the lifetime parameter Γ and the polarization P in the fit without degeneracy. It also seems that in many cases one would need to implement both spin polarization and lifetime effects into the model simultaneously to properly describe the spectra but to do this one would need a way to avoid the possible degeneracy from fitting with multiple added parameters. Bugoslavsky *et al.* [58] have suggested that this could be done by minimizing the variance between the measured and the calculated spectrum.

The most noticeable difference in the behaviour of the fit parameters of the two modified BTK models is the behaviour of the Z parameter. As can be seen in Figures 5.3 and 5.5, in the polarization model the values of the Z parameter are distributed rather evenly between zero and 0.8 while in the lifetime model they are concentrated close to 0.5. There should be physical reasons behind this behaviour.

Previously Woods *et al.* [42] have suggested that in the case of superconductor - half metal Pb-CrO_2 contacts the magnitude of the Z parameter could be used as an indication of the diffusive nature of the contacts. They suggested that $Z \approx 0.5$ could be used as a dividing point between ballistic and diffusive samples so that if all measured spectra have $Z \geq 0.5$ that would indicate diffusivity and contacts with $Z \leq 0.5$ indicate ballistic transport in the contact region [42]. Similar numerical values for the Z parameter have previously been used to describe diffusive spectra with a ballistic model [34, 35]. The analysis of our data with the polarization model produces mainly points with $Z \leq 0.5$ and would place the contacts in the ballistic regime but when the contacts were analysed with the lifetime model the magnitude Z would seem to open a possibility of diffusive transport.

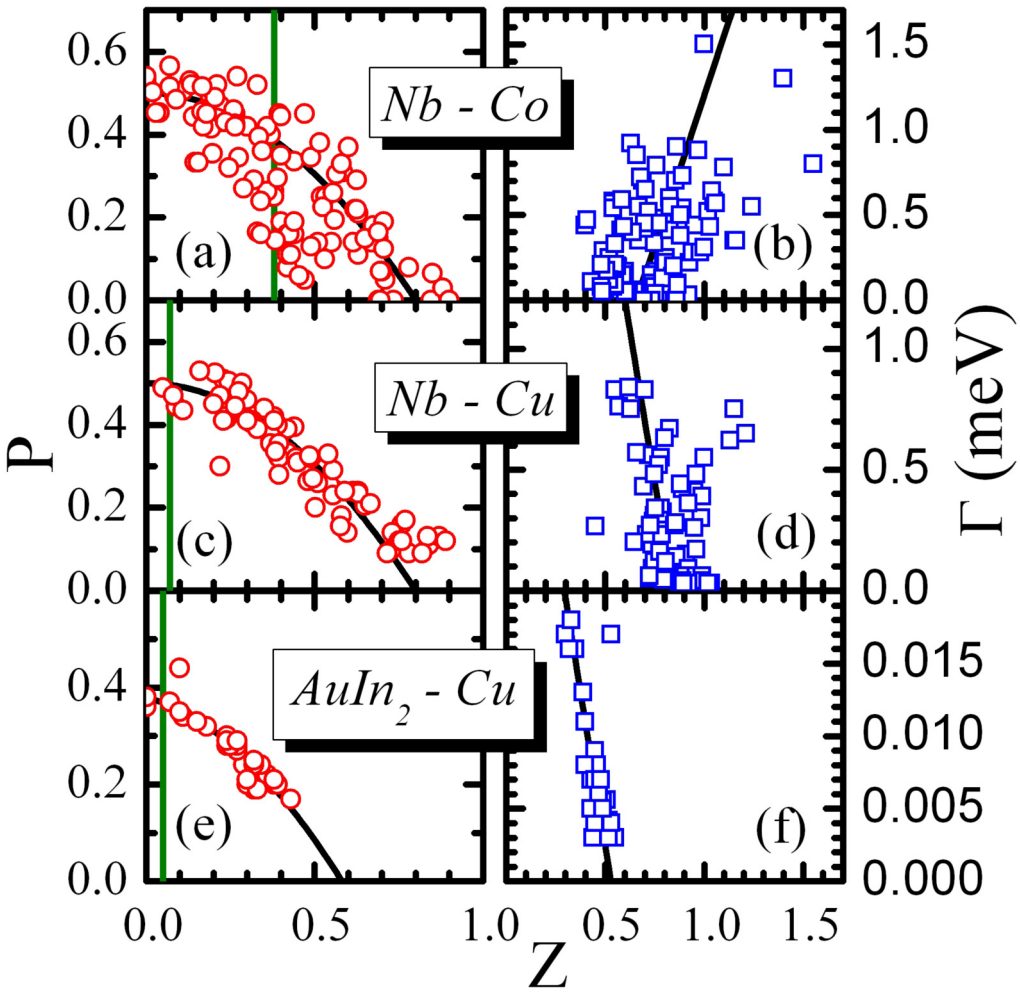

Figure 5.3: Polarization P at $\Gamma = 0$ and lifetime parameter Γ at $P = 0$ as function of the Z parameter for Nb - Co, Nb - Cu and $AuIn_2$ - Cu contacts. The green vertical solid lines on the left represent the expected Z_0 from Fermi surface mismatch. Black solid lines through the data points serve as guide to the eye. [**P1**]

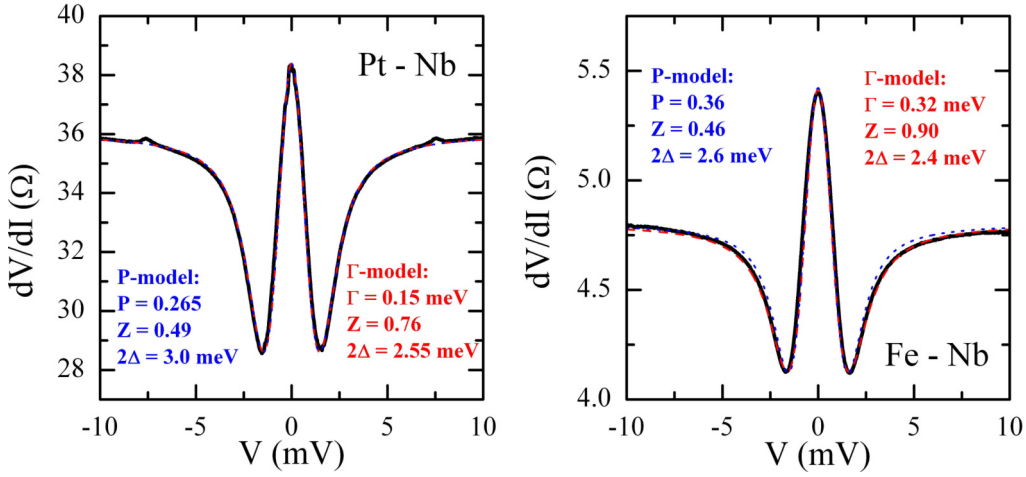

Figure 5.4: Spectra of a Pt - Nb (left) and a Fe - Nb (right) point contact measured in liquid He at 4.2 K. Black lines are the measured spectra, blue dotted lines the fit with the polarization model and red dashed line with the lifetime model. [**P2**]

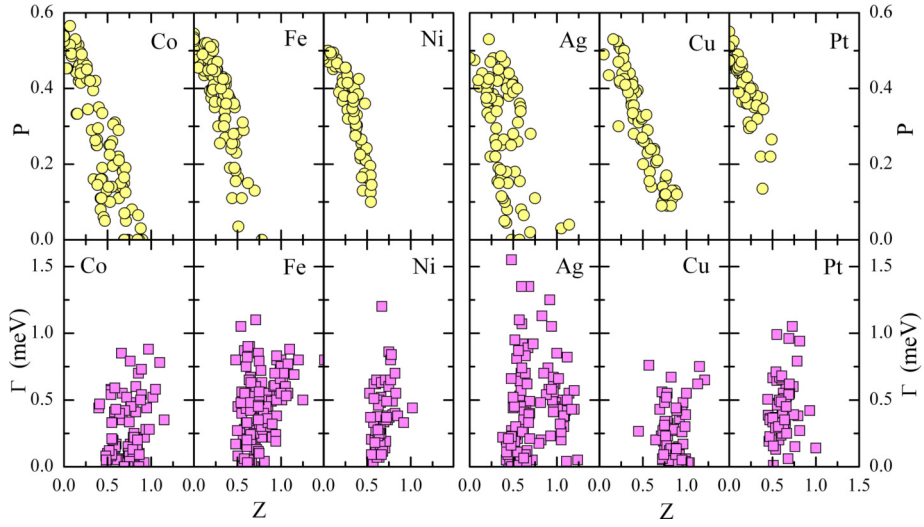

Figure 5.5: The spin polarization P (top) and the lifetime parameter Γ (bottom) as function of the Z parameter for the ferromagnets Co, Fe and Ni and non-magnetic Ag, Cu and Pt in contact with superconducting Nb. The measurements were carried out at 4.2 K. [**P2**]

6. The effect of the Z parameter

In the BTK model the Z parameter describes the strength of the δ function barrier that is used to model the interface potential. It is usually taken to be a phenomenological parameter that either measures the amount of elastic scattering [62] or absorbs the imperfections of the experimental conditions [42].

In the one dimensional BTK model [34], the Z parameter is related to the transmission coefficient τ of the interface

$$\tau = \frac{1}{1+Z^2}\,. \tag{6.1}$$

Our data indicates that we have highly transmissive interfaces. In the polarization model the Z parameter ranges from zero to approximately 0.5 (with some data points up to $Z \approx 1$) which corresponds to transmission coefficients from 1.0 to 0.8 (or down to 0.5 for the few points at higher Z). In the lifetime model the data points are concentrated around $Z \approx 0.5$ corresponding to a transmission coefficient $\tau \approx 0.8$.

Earlier studies on the superconducting proximity effect on thin film systems have investigated the transmission coefficients of small interfaces. There it has been found that the transmission coefficient was close to $\tau \approx 0.3$ for non- magnetic metals in contact with Nb [73]. Current perpendicular to plane magneto-resistance measurements produce similar magnitudes for the transmission coefficients even though the experimental set up should prevent any oxide barriers to be present at the interfaces [73–75].

Early on, it was noted that there are also other sources for reflection than the tunneling barrier at the interface. One of these mechanisms is called Fermi velocity (or surface) mismatch. In an Andreev reflection experiment, the properties of the Fermi surface are in most cases different for the electrodes that form the contact and this difference should lead to normal reflection even in the absence of a dielectric barrier at the interface. This effect shifts the value of the Z parameter higher according to

$$Z^2 = Z_0^2 + \frac{(1-r)^2}{4r} \tag{6.2}$$

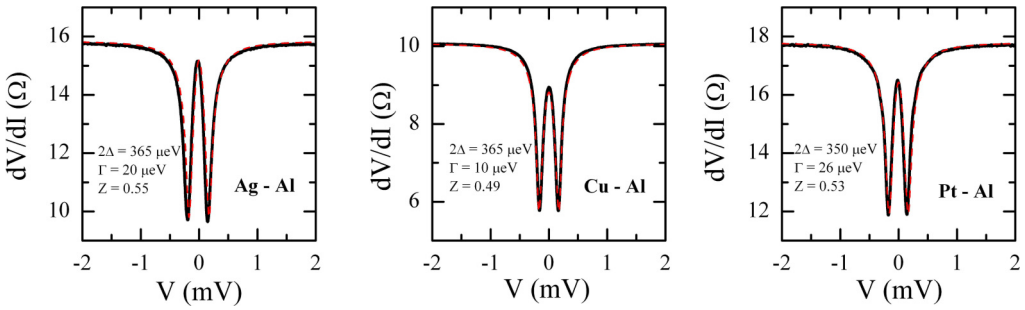

Figure 6.1: Differential resistance spectra (black solid line) of superconducting Al in contact with normal metals Ag, Cu and Pt at 0.1 K in vacuum. The lifetime model fit to the data is shown with the red dashed line. [**P3**]

where Z_0 represents the contribution from the tunneling barrier and r the ratio of the Fermi velocities of the electrodes [62].

We focussed on non-magnetic normal metals when investigating the Z parameter to rule out any interference with the spin polarization. Therefore the spectra were also only fitted with the lifetime model. We performed many measurements below 4.2 K to reduce thermal smearing to a minimum. Many of the low temperature measurements were performed with Al ($T_c = 1.2$ K) as the superconductor instead of or in addition to Nb.

6.1 Normal reflection at superconductor - normal metal interfaces due to Fermi surface mismatch [P3]

Typical spectra of contacts between superconducting Al and normal metals Ag, Cu and Pt measured in vacuum at 0.1 K are shown in Figure 6.1 with corresponding lifetime fits. We found that the values of the Z parameter are concentrated close to 0.5. All of the analysed spectra had roughly the same Z value with both Nb and Al even though the metals have different Fermi surfaces. [**P3**]

To study this accumulation further, we collected the distribution of the Z parameter. All of the Z distributions of Ag, Cu and Pt in contact with both Nb and Al in Figure 6.2 had clear onsets, finite widths and in some cases a weak tail at large Z values. These histograms highlight how similarly the investigated interfaces behave. [**P3**]

We also plotted Z values as function of the contact resistance in normal state R_N to investigate if the size of the contact affects the Z values. This is shown in Figure 6.3 for our spectra with the non-magnets. In this case Z varies only very weakly from 1 to

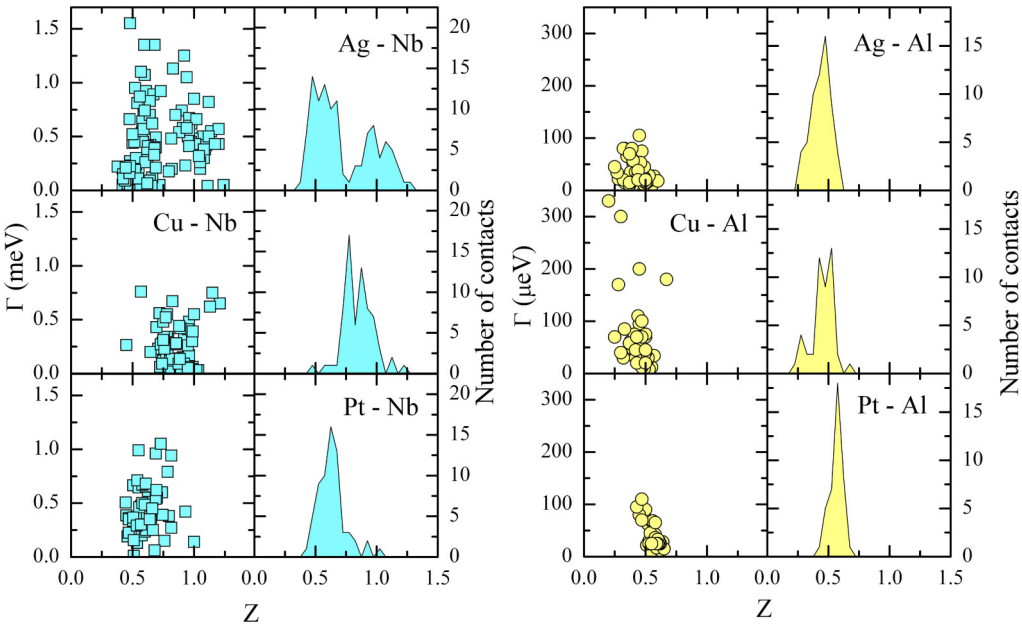

Figure 6.2: The lifetime parameter Γ as function of the strength of the interface barrier Z and the number of contacts at each Z interval for Nb - normal metal contacts measured at 4.2 K and Al - normal metal contacts measured at 0.1 K. [**P3**]

100 Ω. [**P3**]

The magnitude of the lifetime parameter Γ is different for the two investigated superconductors but seems independent of the normal metal. Based on these two superconductors, Γ scales with the critical temperature T_c or the energy gap 2Δ of the superconductor. [**P3**]

6.2 Electron and hole transmission through superconductor - normal metal interfaces [P4]

We measured some spectra at different temperatures from well below the critical temperature of the superconductor to above it, as shown in Figure 6.4 for an Al - Au contact. As shown in the insets of this Figure, the superconducting energy gap $2\Delta(T)$ follows the BCS temperature dependence, while Γ and Z are less affected by the temperature. Because the fit parameters did not depend strongly on the temperature, most of the contacts used in the following analysis were measured only at $T = 0.1$ K well below the critical temperature of Al. [**P4**]

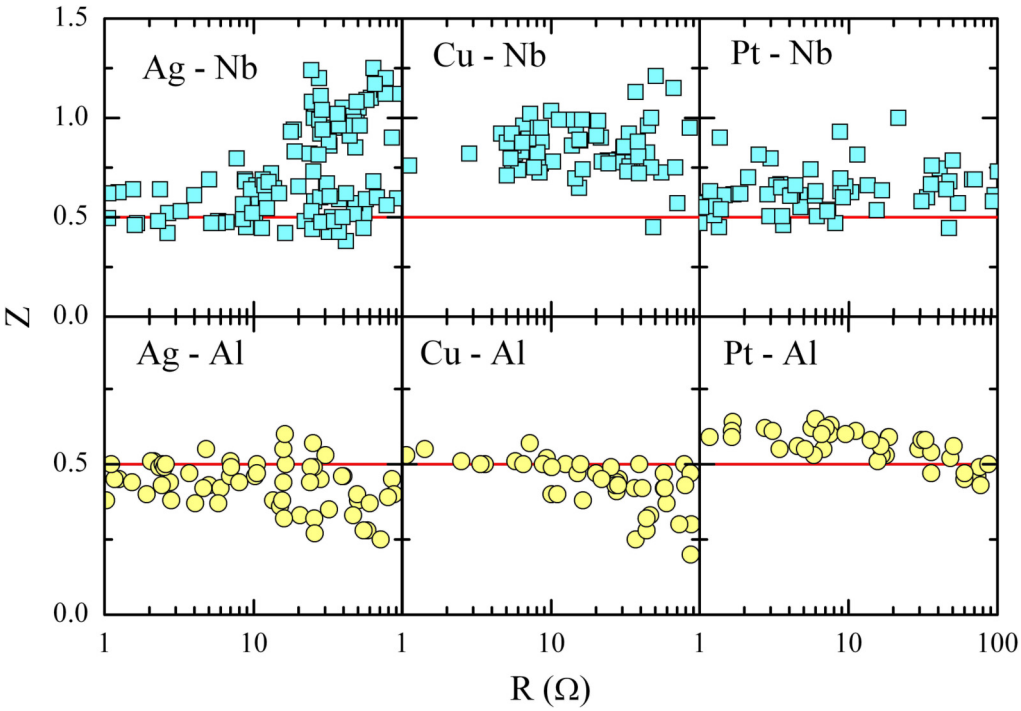

Figure 6.3: The Z parameter as function of the normal state contact resistance R_N for Nb (at 4.2 K) and Al (at 0.1 K) in contact with Ag, Cu and Pt. The red lines at $Z = 0.5$ are drawn as guides to the eye. [**P3**]

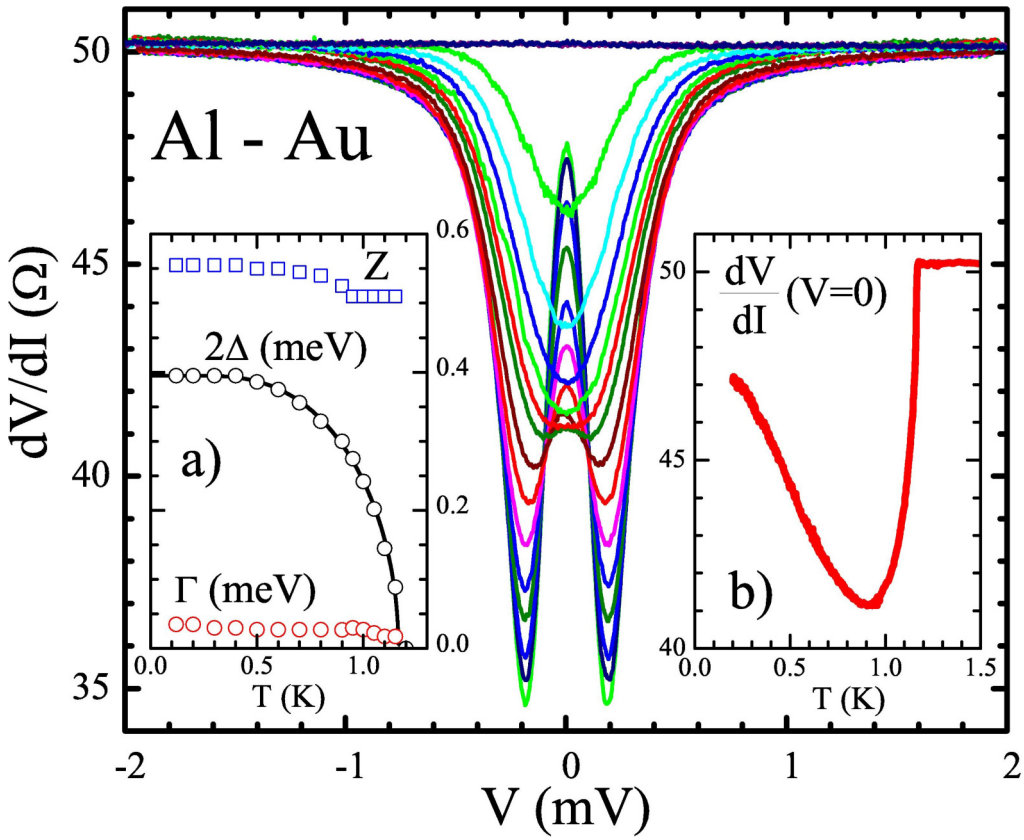

Figure 6.4: Differential resistance spectra of an Al - Au contact. The lowest measuring temperature was 0.1 K and the temperature steps 0.1 K up to 0.9 K and 0.05 K above that. The inset a) shows the temperature dependence of the BTK fit parameters and the inset b) the zero bias resistance measured during cooling. The Z parameter was held constant at temperatures close to the T_c. [**P4**]

Figure 6.5 shows for Al - Au contacts that while the energy gap $2\Delta_0$ and the lifetime parameter Γ rise with increasing resistance, the Z parameter stays constant. The superconducting energy gap stays almost constant close to the literature value of 365 μeV from below 1 Ω up to around 100 Ω. At higher resistances the gap value approximately doubles. In thin films (2D) or wires (1D) the critical temperature T_c has been observed to rise when the size decreases [76, 77]. We have speculated that this could also happen in point contacts (0D) even though it is unlikely that the true material dependent gap would grow as a function of the resistance R. The lifetime parameter Γ seems to have a stronger resistance dependence. For contacts with resistances below 10 Ω, it is close to 10 μeV and of the same order as the thermal smearing. It increases almost linearly between 10 Ω and 100 Ω, and saturates at higher resistances close to 200 μeV. [**P4**]

The Z parameter stays constant at approximately 0.5 for resistances ranging from below 1 Ω to several thousand ohms. In the kiloohm range Z increases when approaching the transition to vacuum tunneling. Similar behaviour is observed also for point contacts between superconducting Al and the normal metals Ag, Cu, Pd, and Pt, as shown for the Z parameter in Figure 6.6. The Z parameter drops slightly close to 100 Ω and increases again at higher contact resistances. This behaviour coincides with the increase of $2\Delta_0$ and the saturation of the lifetime parameter Γ. [**P4**]

6.3 Discussion

According to the free-electron approximation, these metal combinations should have Z values close to zero. Proximity-effect [78, 79] and perpendicular current studies [75, 80, 81] on the other hand yielded Z values closer to one. Our point-contact results do not fit either of the two cases. One could assume that the constant Z could be caused by a tunneling barrier at the interface, but that should lead to stronger variation because the transmission coefficient depends exponentially on the barrier width and height [82]. [**P3**]

The onset of the Z histograms marks the smallest value of the Z parameter which has been reached in our contacts. These points could correspond to contacts with a negligibly small tunnel barrier so that most of the Z arises from the Fermi surface mismatch. If this interpretation of the Z parameter holds, point-contact Andreev reflection spectroscopy might open a way to measure the Fermi surface mismatch between metals. [**P3**]

The same argument used to exclude tunneling as a cause for the uniform Z param-

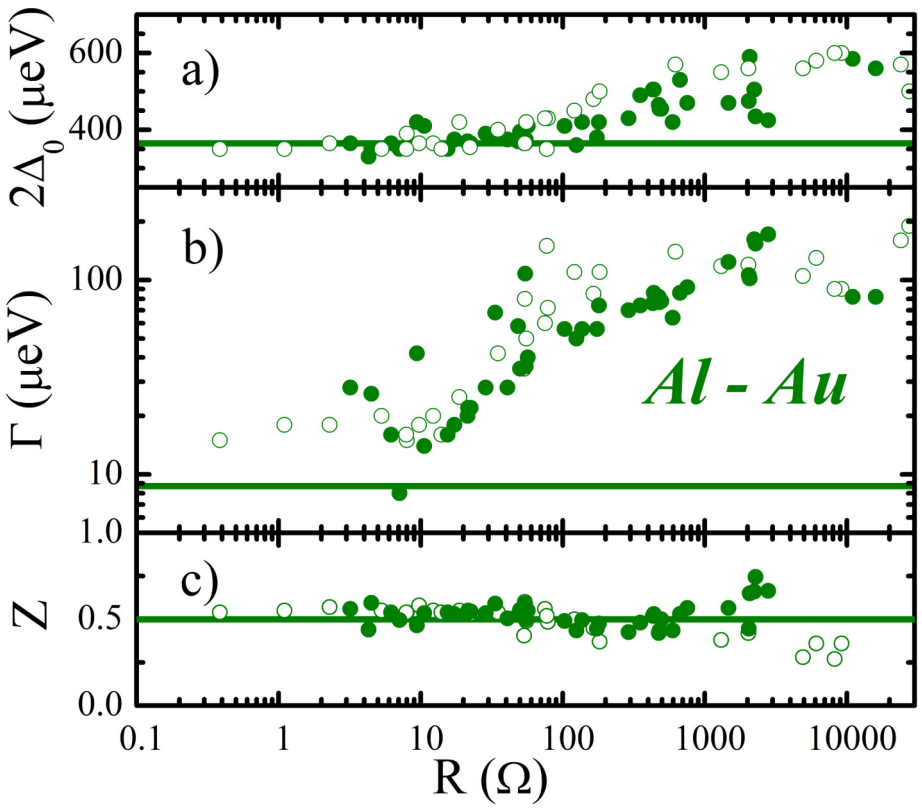

Figure 6.5: The fit parameters of Al-Au contacts from the lifetime model as function of contact resistance R_N at $T = 0.1$ K: a) the superconducting energy gap $2\Delta_0$ (the solid line at 365 μeV is the bulk energy gap of Al), b) the lifetime parameter Γ with the thermal energy k_BT as reference and c) the Z parameter and a line drawn at 0.5 as a guide for the eye. Different measurement series are marked with open and closed symbols. [**P4**]

eter can also be applied to Fermi surface mismatch because it should not cause such an uniform distribution of Z values. Our samples are polycrystalline and therefore crystal directions at the contact interface should vary. This should produce Z parameters of slightly different magnitudes for contacts at different positions on the interfaces. This is not observed in our measurements which implies that the Z is probably not caused by the Fermi surface mismatch. [**P4**]

The reflection from a tunnel barrier should be a probabilistic process and both the incident electrons and retro-reflected holes are equally affected. Fermi surface mismatch on the other hand is selective with respect to the wave number and angle of incidence which means that the retro-reflected holes should not be affected. This is because the

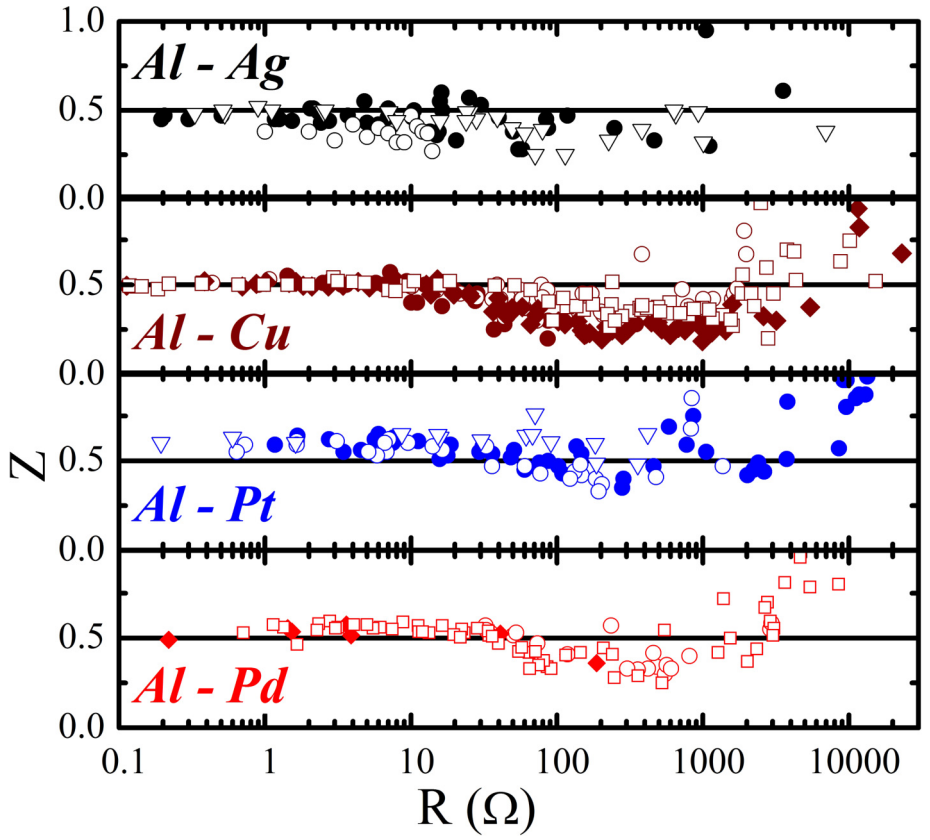

Figure 6.6: The Z parameter as function of the normal resistance R_N of Al in contact with the non-magnetic metals Ag, Cu, Pt and Pd at the temperature of $T = 0.1$ K. The solid lines are drawn at $Z = 0.5$ as guide to the eyes. The different symbols mark measurement series. [**P4**]

Andreev reflection process ensures that they have the same - or almost the same - properties as the incident electrons that have already crossed the interface. If this is correct, Andreev reflection should not be affected by the Fermi surface mismatch and it can not be resolved with Andreev-reflection spectroscopy. [**P4**]

7. Polarization measurements at lower temperatures

7.1 Spin polarization and suppression of superconductivity at nanoscale ferromagnet - superconductor interfaces [P5]

To minimize broadening caused by the temperature, and to investigate how the BTK parameters behave at lower temperatures, we measured a number of spectra of contacts between ferromagnetic Fe and superconductors Nb ($T_c = 9.2$ K), Ta ($T_c = 4.3$ K), Sn ($T_c = 3.7$ K), Al ($T_c = 1.2$ K) and Zn ($T_c = 0.88$ K) at temperatures down to 0.1 K and below. We measured the differential resistance dV/dI as function of voltage V at different temperatures T ranging from well below the critical temperature of the superconductor to above it. After that the contact was cooled back to the lowest temperatures and the resistance at zero bias $R(T)$ was recorded as function of temperature. The spectra were analysed with Strijkers' model [18]. [**P5**]

At the lowest measuring temperatures, most of the spectra had the typical double minimum structure of Andreev reflection (Figures 7.1-7.4). Despite this, the critical temperatures were greatly reduced, especially for contacts with Sn (up to 10 %) and Al (up to 40 %). These features are often more clearly visible in the temperature dependence of the zero-bias resistance $R(T)$. Most contacts with Nb and Ta, the superconductors with the highest critical temperatures, had a T_c close to the expected bulk value and the $R(T)$ varied smoothly below that. The $R(T)$ for contacts with Sn and Al (Figure 7.2) showed a transition from superconducting to normal state well below the bulk critical temperature of the elements. Some of the spectra with Al, Sn and Ta had two critical temperatures (Figure 7.3). The second transition would arise from a layer with a lower critical temperature in the contact region caused by the local field of the ferromagnet. The resistance drop and temperature at these transitions varied from

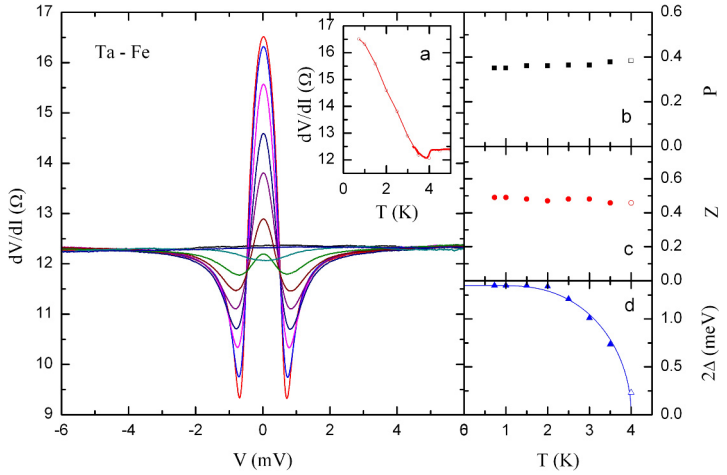

Figure 7.1: Differential resistance dV/dI versus bias voltage V of a Ta - Fe contact. The lowest two temperatures were 0.73 K and 1.0 K. Above that the temperature was increased in steps of 0.5 K up to 5.0 K. The Inset a) The temperature dependence of the contact resistance R at zero bias measured during cool down, and the side panels show the BTK fit parameters b) the polarization P, c) the Z parameter and d) the superconducting gap 2Δ. The BCS curve has been drawn with $T_c = 4.0$ K. [**P5**]

contact to contact. For example, the observed critical temperature of Al contacts varied from 0.75 K to 1.2 K. For the superconductor with the lowest critical temperature, Zn, we measured spectra that were so strongly reduced in magnitude that they had to be scaled to be fitted with the BTK model while others could be fitted without scaling (Figure 7.4). The scaling parameter x varied typically from 0.5 to 0.8. [**P5**]

The typical three-parameter BTK fit with P, Z and 2Δ as parameters describes most of the spectra rather well. As the side panels in Figures 7.1- 7.4 show, the superconducting energy gap follows the BCS curve and the Z parameter and spin polarization P do not depend on temperature (within error bars). At the lowest temperatures the error bars were smaller than the symbol size. At higher temperatures the error bars grow because the spectral features become more washed out, and this variation from one temperature to another is larger than the uncertainty at the lowest temperatures. This scattering could be related to the changing magnetic field, tiny changes in the contact or slight instability of the temperature. The Z dependence of polarization (Figure 7.5), as well as the extrapolated polarization $P(Z = 0)$, agree both with literature data [18] and our earlier measurements with Nb at 4.2 K [**P2**]. [**P5**]

The scaling needed to fit the strongly reduced Zn spectra was modelled as a partly

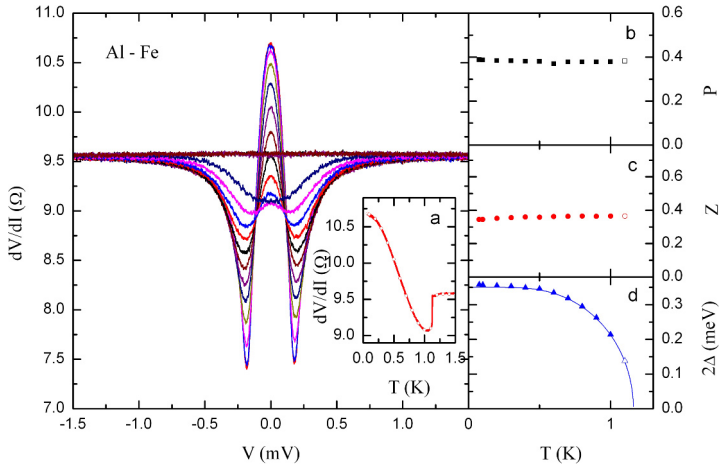

Figure 7.2: Differential resistance dV/dI versus bias voltage V of an Al - Fe contact from 0.075 K to 1.4 K. The lowest two temperatures are 0.075 K and 0.10 K. Above that the temperature increases in steps of 0.1 K. Inset a) The temperature dependence of the contact resistance R at zero bias. The side panels show the temperature dependence of the BTK fit parameters b) the polarization P, c) the Z parameter and d) the superconducting gap 2Δ. The BCS curve is drawn with a critical temperature of 1.2 K. [**P5**]

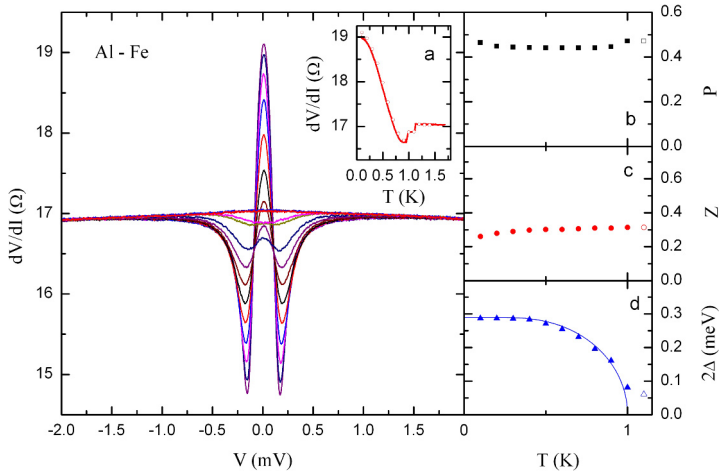

Figure 7.3: Differential resistance dV/dI as function of the bias voltage V of an Al - Fe contact from 0.1 K to 1.4 K in steps of 0.1 K. Insets: a) The temperature dependence of the contact resistance R at zero bias (solid red line) together with values extracted from the spectra (open circles). Side panel: The temperature dependence of the BTK fit parameters b) polarization P , c) Z and d) the superconducting gap 2Δ. The BCS curve is drawn with a critical temperature of 1.0 K and no additional broadening was included in this analysis.

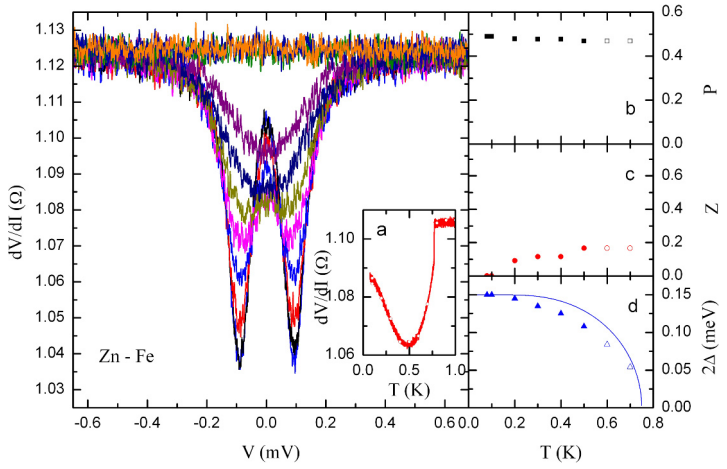

Figure 7.4: Differential resistance dV/dI versus bias voltage V of a Zn - Fe contact from 0.1 K to 1.0 K in steps of 0.1 K. The inset a) shows the temperature dependence of the contact resistance R at zero bias with the bulk T_c indicated and the side panels show b) the polarization, c) the normal reflection coefficient Z, and d) the superconducting energy gap 2Δ. [**P5**]

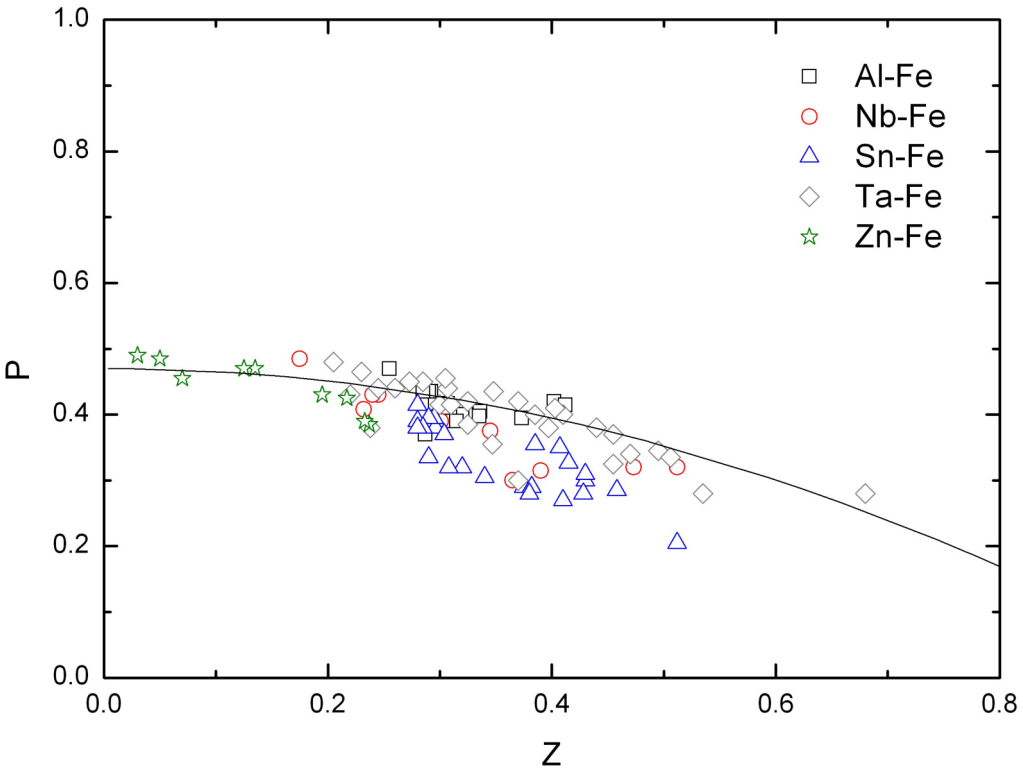

Figure 7.5: The polarization P from the three-parameter BTK model as function of the Z parameter at the lowest measuring temperatures for superconductors Nb (red circles), Ta (grey diamonds), Sn (blue triangles), Al (black squares) and Zn (green stars) in contact with Fe. The black solid line $P(Z) = 0.47(1 - Z^2)$ is a guide to the eye.

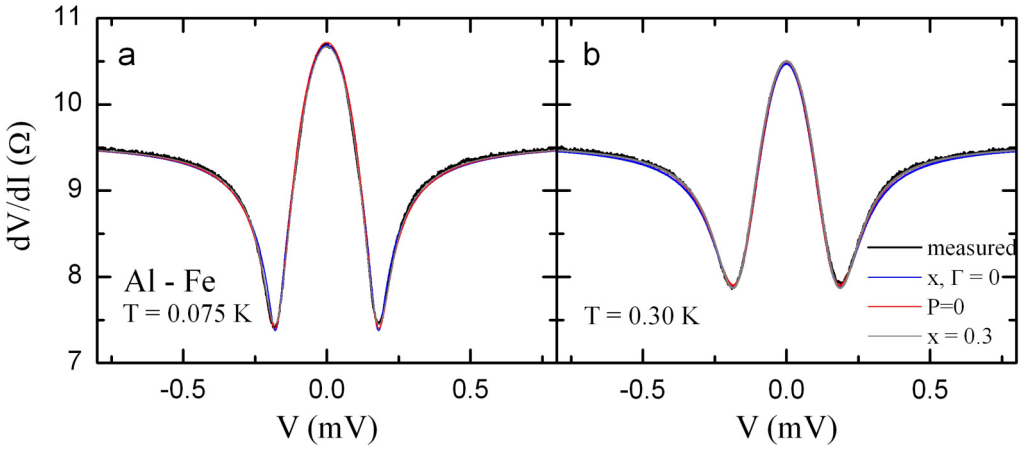

Figure 7.6: Measured spectra (solid black line) and fit curves with the three-parameter model with P, Z and 2Δ as fit parameters (blue), the scaling model with lifetime broadening without polarization (red), and an optimum fit with the scaling model and thermal broadening (grey) for the Al-Fe contact of Figure 7.2 at a) the lowest measuring temperature of 0.075 K and b) 0.30 K. The x is the scaling parameter of the scaling model. [**P5**].

normal contact interface, which adds another fitting parameter, the normal fraction of the contact area x, into the BTK model. In addition to the scaling factor x the model contained either thermal or lifetime broadening. The thermal broadening is included by replacing the measuring temperature T by an effective temperature $T + \omega/k$ where ω is called the thermal broadening parameter. The same scaling can also be used to analyse the other spectra for which the fitting could be performed without scaling. When the fitting quality was monitored with the standard deviation χ, the model with thermal broadening in addition to the scaling factor produced smallest deviations with respect to the measured spectra. Both broadening mechanisms lead to a reduced polarization and an increased Z parameter. With lifetime broadening the spectra can in the extreme case be fitted completely without polarization, as Figure 7.6 shows for the Al-Fe contact of Figure 7.2. [**P5**]

7.2 Discussion

We speculate that the variation of the spectral features could be related to the inhomogeneous magnetic field created by the Fe wire. The spectra of contacts with the superconductors with the highest critical fields are affected the least, and the ones with the

superconductors with the lowest critical temperatures are affected the most. To cause the observed spectra with reduced magnitude and critical temperatures, the maximum value of the magnetic field of the Fe wire should be close to $B_{Fe} \approx 10$ mT. Even though this field is larger than the critical field of Zn, the magnetic field is so localized that it only affects a small volume near the contact interface so that further away from the contact interface the superconductor remains superconducting and contributes to Andreev reflection. [**P5**]

When the spectra are fitted with a finite scaling factor x, the extracted polarization drops and the Z parameter increases closer to the values observed when contacts with non-magnetic metals are analysed with the lifetime model. This essentially follows the $P(Z)$ dependence of the three-parameter model. With lifetime broadening, the spin polarization is strongly reduced, even down to zero. Fitting with thermal broadening on the other hand results in a smaller standard deviation and a smaller drop of spin polarization than with the lifetime broadening. The broadening parameters ω and Γ of both models $\sim 10\mu$eV are of the same order of magnitude with the thermal energy at the lowest measuring temperature and at least an order of magnitude lower than the kinetic energy of electrons at the gap edge. [**P5**]

8. Conclusions

We have measured point-contact Andreev reflection spectra between a number of superconductors and both non-magnetic and ferromagnetic metals. With superconducting Nb at 4.2 K the spectra of both non-magnets and ferromagnets can be interpreted in two completely different ways, either with spin polarization or with the finite lifetime of Cooper pairs. The analysis with the polarization model reproduced the $P(Z)$ dependence and the magnitude of the extracted spin polarization in agreement with the literature data. With the lifetime model on the other hand, the Z parameter is nearly constant at $Z \approx 0.5$ while the polarization is set to zero.

At lower temperatures the dualism seems to be partly resolvable because of the reduced amount of thermal broadening. Measurements at lower temperatures with non-magnetic metals found a nearly constant Z parameter for all investigated metal combinations. With the of ferromagnetic metals the polarization at low temperatures matches that measured at 4.2 K. However, the temperature dependence of the spectra revealed more anomalies than could have been found at a fixed temperature, including reduced critical temperatures or two superconducting transitions. We have speculated that this could be attributed to the inhomogeneous magnetic field of the ferromagnetic wire that would suppress the superconductivity in the contact region. We have modelled the reduced superconducting signal by introducing a scaling factor. In turn, this new fit parameter can also lead to an ambiguous interpretation similar to the polarization-lifetime ambiguity found for the Nb contacts measured at 4.2 K.

A method for distinguishing the right interpretation is needed. We have attempted to use the normal reflection as a separating criterion but because the origin of the constant Z of the lifetime model is still unclear it is difficult to obtain enough physical information needed for such a selection.

Bibliography

[1] Y. Naidyuk and I. K. Yanson, *Point-Contact Spectroscopy* (Springer, 2005).

[2] A. G. M. Jansen, A. P. van Gelder, and P. Wyder, J. Phys. C: Solid State Phys. **13**, 6073 (1980).

[3] A. M. Duif, A. G. M. Jansen, and P. G. Wyder, J. Phys.: Condens. Matter. **1**, 3157 (1989).

[4] K. Gloos, Low Temp. Phys. **35**, 935 (2009), [Fiz. Nizk. Temp. **35** 1204].

[5] K. Gloos and E. Tuuli, J. Phys.: Conf. Ser. **400**, 042011 (2012).

[6] G. A. Prinz, Physics Today **48**, 58 (1995).

[7] S. A. Wolf, D. D. Awschalom, R. A. Buhrman, J. M. Daughton, S. von Molnár, M. L. Roukes, A. Y. Chtchelkanova, and D. M. Treger, Science **294**, 1488 (2001).

[8] I. Žutić, J. Fabian, and S. Das Sarma, Rev. Mod. Phys. **76**, 323 (2004).

[9] J. Sinova and I. Žutić, Nature Materials **11**, 368 (2012).

[10] C. Kittel, *Introduction to Solid State Physics*, fourth edition ed. (John Wiley & Sons, Inc., 1971).

[11] I. I. Mazin, Phys. Rev. Lett. **83**, 1427 (1999).

[12] P. A. Dowben, N. Wu, and C. Binek, J. Phys.: Condens. Matter **23**, 171001 (2011).

[13] G. Busch, M. Campagna, and H. C. Siegmann, Phys. Rev. B **4**, 746 (1971).

[14] G. Busch, M. Campagna, P. Cotti, and H. C. Siegmann, Phys. Rev. Lett. **22**, 597 (1969).

[15] R. Meservey and P. M. Tedrow, Phys. Rep. **238**, 173 (1994).

[16] R. J. Soulen, J. M. Byers, M. S. Osofsky, B. Nadgorny, T. Ambrose, S. F. Cheng, P. R. Broussard, C. T. Tanaka, J. Nowak, J. S. Moodera, A. Barry, and J. M. D. Coey, Science **282**, 85 (1998).

[17] M. J. M. de Jong and C. W. J. Beenakker, Phys. Rev. Lett. **74**, 1657 (1995).

[18] G. J. Strijkers, Y. Ji, F. Y. Yang, C. L. Chien, and J. M. Byers, Phys. Rev. B **63**, 104510 (2001).

[19] R. Feder, ed., "Polarized electrons in surface physics," (World Scientific Publishing Co. Pte. Ltd., 1985) Chap. 5. Sources and Detectors for Polarized Electrons, pp. 265–271.

[20] I. Giaever, Phys. Rev. Lett. **5**, 147 (1960).

[21] I. Giaever, Phys. Rev. Lett. **5**, 464 (1960).

[22] P. M. Tedrow and R. Meservey, Phys. Rev. Lett. **26**, 192 (1971).

[23] P. M. Tedrow and R. Meservey, Phys. Rev. B **7**, 318 (1973).

[24] R. Meservey, P. M. Tedrow, and P. Fulde, Phys. Rev. Lett. **25**, 1270 (1970).

[25] J. J. Pankove, Phys. Lett. **21**, 406 (1966).

[26] A. G. M. Jansen, F. M. Mueller, and P. Wyder, Phys. Rev. B **16**, 1325 (1977).

[27] N. Agraït, A. Levy Yeyati, and J. M. van Ruitenbeek, Phys. Rep. **377**, 81 (2003).

[28] Y. V. Sharvin, Sov. Phys. - JETP **21**, 655 (1965).

[29] F. Kohlrausch, Ann. Phys., Lpz. **1**, 132 (1900).

[30] A. Andreev, Sov. Phys. JETP **19**, 1228 (1964), [Zh. Eksp. Teor. Fiz. 46, 1823 (1964)].

[31] P. G. de Gennes and D. Saint-James, Phys. Lett. **4**, 151 (1963).

[32] S. K. Upadhyay, A. Palanisami, R. N. Louie, and R. A. Buhrman, Phys. Rev. Lett. **81**, 3247 (1998).

[33] Y. Ji, G. J. Strijkers, F. Y. Yang, and C. L. Chien, Phys. Rev. B **64**, 224425 (2001).

[34] G. E. Blonder, M. Tinkham, and T. M. Klapwijk, Phys. Rev. B **25**, 4515 (1982).

[35] I. I. Mazin, A. A. Golubov, and B. Nadgorny, J. Appl. Phys. **89**, 7576 (2001).

[36] P. Chalsani, S. K. Upadhyay, O. Ozatay, and R. A. Buhrman, Phys. Rev. B **75**, 094417 (2007).

[37] F. Pérez-Willard, J. C. Cuevas, C. Sürgers, P. Pfundstein, J. Kopu, M. Eschrig, and H. v. Löhneysen, Phys. Rev. B **69**, 140502 (2004).

[38] S. Mukhopadhyay, P. Raychaudhuri, D. A. Joshi, and C. V. Tomy, Phys. Rev. B **75**, 014504 (2007).

[39] B. Nadgorny, I. I. Mazin, M. Osofsky, R. J. Soulen, P. Broussard, R. M. Stroud, D. J. Singh, V. G. Harris, A. Arsenov, and Y. Mukovskii, Phys. Rev. B **63**, 184433 (2001).

[40] C. H. Kant, O. Kurnosikov, A. T. Filip, P. LeClair, H. J. M. Swagten, and W. J. M. de Jonge, Phys. Rev. B **66**, 212403 (2002).

[41] Y. Miyoshi, Y. Bugoslavsky, and L. F. Cohen, Phys. Rev. B **72**, 012502 (2005).

[42] G. T. Woods, R. J. Soulen, I. Mazin, B. Nadgorny, M. S. Osofsky, J. Sanders, H. Srikanth, W. F. Egelhoff, and R. Datla, Phys. Rev. B **70**, 054416 (2004).

[43] J. P. DeGrave, A. L. Schmitt, R. S. Selinsky, J. M. Higgins, D. J. Keavney, and S. Jin, Nano Letters **11**, 4431 (2011).

[44] B. Nadgorny, M. S. Osofsky, D. J. Singh, G. T. (Woods, R. J. Soulen, M. K. Lee, S. D. Bu, and C. B. Eom, Appl. Phys. Lett. **82**, 427 (2003).

[45] K. A. Yates, A. J. Behan, J. R. Neal, D. S. Score, H. J. Blythe, G. A. Gehring, S. M. Heald, W. R. Branford, and L. F. Cohen, Phys. Rev. B **80**, 245207 (2009).

[46] F. Rigato, S. Piano, M. Foerster, F. Giubileo, A. M. Cucolo, and J. Fontcuberta, Phys. Rev. B **81**, 174415 (2010).

[47] A. D. Naylor, G. Burnell, and B. J. Hickey, Phys. Rev. B **85**, 064410 (2012).

[48] R. P. Panguluri, K. C. Ku, T. Wojtowicz, X. Liu, J. K. Furdyna, Y. B. Lyanda-Geller, N. Samarth, and B. Nadgorny, Phys. Rev. B **72**, 054510 (2005).

[49] M. S. Osofsky, L. Cheng, W. E. Bailey, K. Bussmann, and D. Parker, Appl. Phys. Lett. **102**, 212412 (2013).

[50] S. V. Karthik, T. M. Nakatani, A. Rajanikanth, Y. K. Takahashi, and K. Hono, J. Appl. Phys. **105**, 07C916 (2009).

[51] I. Shigeta, O. Murayama, T. Hisamatsu, A. Brinkman, A. A. Golubov, Y. Tanaka, M. Ito, H. Hilgenkamp, and M. Hiroi, J. Phys. and Chem. of Solids **72**, 604 (2011).

[52] I. Shigeta, O. Murayama, T. Hisamatsu, M. Ito, and M. Hiroi, Physica C **470**, S806 (2010).

[53] L. Ritchie, G. Xiao, Y. Ji, T. Y. Chen, C. L. Chien, M. Zhang, J. Chen, Z. Liu, G. Wu, and X. X. Zhang, Phys. Rev. B **68**, 104430 (2003).

[54] I. Shigeta, Y. Maeda, K. Harumori, Y. Nishisako, M. Ito, T. Yamauchi, and M. Hiroi, IEEE Trans. Magn. **50**, 1401304 (2014).

[55] J. S. Parker, S. M. Watts, P. G. Ivanov, and P. Xiong, Phys. Rev. Lett. **88**, 196601 (2002).

[56] T. Löfwander, R. Grein, and M. Eschrig, Phys. Rev. Lett. **105**, 207001 (2010).

[57] C. S. Turel, I. J. Guilaran, P. Xiong, and J. Y. T. Wei, Appl. Phys. Lett. **99**, 192508 (2011).

[58] Y. Bugoslavsky, Y. Miyoshi, S. K. Clowes, W. R. Branford, M. Lake, I. Brown, A. D. Caplin, and L. F. Cohen, Phys. Rev. B **71**, 104523 (2005).

[59] V. Baltz, A. D. Naylor, K. M. Seemann, W. Elder, S. Sheen, K. Westerholt, H. Zabel, G. Burnell, C. H. Marrows, and B. J. Hickey, J. Phys.: Condens. Matter **21**, 095701 (2009).

[60] J. A. Gifford, C. N. Snider, J. Martinez, and T. Y. Chen, J. Appl. Phys. **113**, 17B105 (2013).

[61] A. Plecenník, M. Grajcar, v. Beňačka, P. Seidel, and A. Pfuch, Phys. Rev. B **49**, 10016 (1994).

[62] G. E. Blonder and M. Tinkham, Phys. Rev. B **27**, 112 (1983).

[63] K. Xia, P. J. Kelly, G. E. W. Bauer, and I. Turek, Phys. Rev. Lett. **89**, 166603 (2002).

[64] N. W. Ashcroft and N. D. Mermin, *Solid State Physics* (Thomson Learning, 1976).

[65] M. Tinkham, *Introduction to Superconductivity* (Dover Publications, Inc., 2004).

[66] L. N. Cooper, Phys. Rev. **104**, 1189 (1956).

[67] J. Bardeen, L. N. Cooper, and J. R. Schrieffer, Phys. Rev. **108**, 1175 (1957).

[68] R. C. Dynes, V. Narayanamurti, and J. P. Garno, Phys. Rev. Lett. **41**, 1509 (1978).

[69] R. C. Dynes, J. P. Garno, G. B. Hertel, and T. P. Orlando, Phys. Rev. Lett. **53**, 2437 (1984).

[70] H. Srikanth and A. K. Raychaudchuri, Physica C **190**, 229 (1992).

[71] Y. de Wilde, T. M. Klapwijk, A. Jansen, J. Heil, and P. Wyder, Physica B **218**, 165 (1996).

[72] K. Gloos and F. Martin, Z. Phys. B - Condens. Matter **99**, 321 (1996).

[73] A. Tesauro, A. Aurigemma, C. Cirillo, S. L. Prischepa, M. Salvato, and C. Attanasio, Supercond. Sci. Technol. **18**, 1 (2005).

[74] W. Park, D. V. Baxter, S. Steenwyk, I. Moraru, W. P. Pratt Jr., and J. Bass, Phys. Rev. B **62**, 1178 (2000).

[75] A. Sharma, J. A. Romero, N. Theodoropoulou, R. Loloee, W. P. Pratt Jr., and J. Bass, J. Appl. Phys. **102**, 113916 (2007).

[76] S. Matsuo, H. Sugiura, and S. Noguchi, J. Low Temp. Phys. **15**, 481 (1974).

[77] K. Y. Arutyunov, D. S. Golubev, and A. D. Zaikin, Phys. Rep. **464**, 1 (2008).

[78] C. Attanasio, "Nanoscale devices - fundamentals and applications," (Springer, 2006) p. 241.

[79] V. N. Kushnir, S. L. Prischepa, C. Cirillo, and C. Attanasio, J. Appl. Phys. **106**, 113917 (2009).

[80] W. Pratt Jr. and J. Bass, Appl. Surf. Sci. **256**, 399– (2009).

[81] A. Sharma, N. Theodoropoulou, S. Wang, K. Xia, W. P. Pratt, and J. Bass, J. Appl. Phys. **105**, 123920 (2009).

[82] J. G. Simmons, J. Appl. Phys. **35**, 2655 (1965).